GeoScienceWorld
Lithosphere
Volume 2022, Article ID 6367642, 24 pages
https://doi.org/10.2113/2022/6367642

Lithosphere

Research Article

Three-Dimensional Stochastic Distribution Characteristics of Void Fraction in Longwall Mining-Disturbed Overburden of Inclined Coal Seam

Shaofeng Wang,[1,2] **Kanghui Liu**,[1,2] **Zizi Pi**,[1] **Fuchao Tian**,[1,2] **and Yalan Yang**[1]

[1]*School of Resources and Safety Engineering, Central South University, Changsha, Hunan 410083, China*
[2]*State Key Laboratory of Coal Mine Safety Technology, China Coal Technology & Engineering Group Shenyang Research Institute, Shenfu Demonstration Zone 113122, China*

Correspondence should be addressed to Zizi Pi; zizipi@csu.edu.cn

Received 30 April 2022; Accepted 14 June 2022; Published 27 June 2022

Academic Editor: Xiaoding Xu

Fractures in the overburden induced by mining disturbances provide a channel for fluid flow between the surface and the underground. Mining-induced strata movement and fracture distribution are influenced by the gravity and dip angles of rock seams. In this paper, a new three-dimensional theoretical distribution model for void fraction in each partition of overlying rock strata disturbed by inclined coal seam mining was constructed. Based on the theoretical determination model, the three-dimensional random distribution characteristics for void fraction were obtained by combining the random distribution law of void fraction obtained by similar physical simulation experiments and image processing techniques. Theoretical deterministic models, stochastic theoretical models, and similar physical simulations all show that void fraction distribution in the tendency direction of the coal seam shows a bimodal asymmetric distribution with high and low peaks and a symmetric distribution in the strike direction. The void fraction of the overburden in the central part of the mining area is smaller than that of the surrounding area. The results of the theoretically determined model and stochastic model of the void fraction for the strata with different mining lengths and different coal seam inclinations were compared with the results of similar simulation experiments, respectively. The results are in agreement, further verifying the practicality of the model.

1. Introduction

The inclined coal seam mines are numerous and widely distributed in China. Coal seams can be divided into four categories according to their inclination size, as shown in Table 1. The reserves of sharply inclined coal seam account for about 10% to 20% of the total coal reserves [1, 2]. As shown in Figure 1, more than 50% of the mines in the western part of China are mining rapidly inclined coal seams [3]. Therefore, the mining of inclined coal seam occupies a large proportion in the mining of coal seam, and longwall mining is one of the most extensively used mining methods when mining inclined coal seams [4–11]. While mining inclined coal seams, as the mining working face advances, the extent of the mined-out area increases, and the exposed area of the direct top increases, breaking the stress balance of the overlying strata. Redistributing the strata stress and deformation field causes the strata to move in a direction favorable to the equilibrium, resulting in the overlying strata breaking, sinking, and collapsing, and variabilities in the movements and rotations between the overlying strata produce many cracks [12–17]. The damage of the overlying strata has obvious zoning, which can be divided into caved zones, bed separation zones, and ground subsidence zones [18–20]. These fractures include voids between the debris in the caved zone, fractures in the bed separation zone, and fractures in the ground subsidence zone. The fractures provide channels for the flow of subsurface fluids, increasing the mobility of subsurface fluids and the flow of various gases, such as oxygen, smoke, gas; liquids, such as water; and heat transfer. This will result in underground fires in coal mines, groundwater inflow, and gas protrusion and also facilitate the gas

Table 1: Coal seam classification.

Classification basis	Inclination characteristics	Coal seam categories
According to the coal seam inclination	<8°	Approximate horizontal coal seam
	8°-25°	Gradually inclined coal seam
	25°-45°	Inclined coal seam
	>45°	Rapidly inclined coal seam

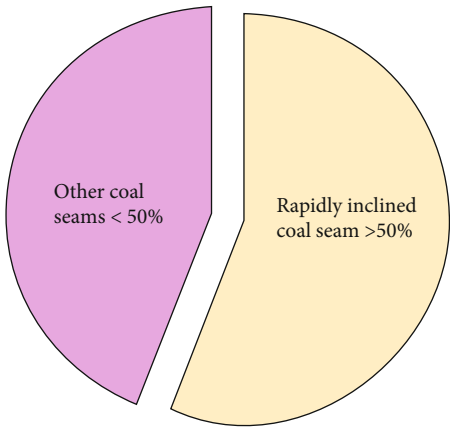

Figure 1: Coal seam mining in the western mining areas of China.

extraction by pressure relief, as shown in Figure 2 [21–25]. Thus, it is important to understand the distribution characteristics of the overburden void fractions disturbed by longwall mining of inclined coal seam to ensure safe and efficient mining in coal mines.

Many scholars at home and abroad have researched in a series of the movement and rupture of overlying strata in inclined coal seam mining. Some scholars have studied the fracture development characteristics in mining-disturbed overburden using field detection and analysis methods [26–28]. Applied borehole TV observation, segmented water injection borehole, distributed fiber optic sensing technology, and microseismic monitoring technology detect the overburden rock rupture height during the working face mining process and determine the rock integrity and fracture development of the overburdened rock in the mined-out area [29–31]. The relationship between ground settlement, the distribution and development patterns of surface cracks, and the widths and depths of cracks were studied by using integrated monitoring methods such as unmanned aerial vehicles, ground-penetrating radar, real-time kinematics, and manual measurements [32, 33]. Although on-site detection can obtain first-hand reliable data, but to monitor the acquisition in real time, which takes a long time and is costly, is not always the best approach. Some scholars have also used theoretical analysis, similar simulation tests, and numerical simulation to study the characteristics of overburden fracture subsidence and mining fracture evolution in inclined coal seam mining [34–39]. Based on the key stratum theory, the annular fracture ring theory and the bicircle theory of the coal seam roof were proposed to evaluate mining fracture evolution. The fracture evolution characteristics, displacement changes, and movement characteristics of the overburdened rock in coal mining work were studied [39, 40]. Sun et al. [41] analyzed the effects of coal seam inclination on the evolution of the overburdened fracture unloading gas transmission channel in the main mining face through physically similar simulation tests and numerical simulations. Liu et al. [42] used numerical simulation to study fracture field evolutions in near-inclined coal seams to fully understand the evolution and distribution characteristics of overburden during coal mining. An energy-absorbing anchor cable is proposed to control the creation and development of cracks in the roof to maintain its stability [43, 44]. Movement and damage of the overburden in inclined coal seam mining can also be influenced by the angle of inclination. The discrete element numerical method was used to study the damage behavior in the roofs of inclined coal seams, determine the relationship between the inclination angle of coal seam and the degree of roof collapse, and obtain the law of roof collapse of inclined coal seam [45]. Yun et al. [11] investigated the dynamic movement characteristics of multisegment topping coal mining along the strike seam in a large inclined extra thick coal seam. These studies have achieved positive results in terms of the movement and fracture regulation and fracture evolution characteristics of the overburden rock seams overlying the longwall mining of inclined coal seams, but they primarily focus on the movement of the overburdened rock and fracture evolution characteristics, with less research focusing on the fracture quantification and even less research on the three-dimensional distribution state of void fraction generated by rock seam fracture movement.

Additionally, the stability of the rock mass is affected by complex stress perturbations [46, 47]. While mining of inclined coal seams, mining parameters, such as longwall face advancement speed, longwall face length and width, mining height, mining sequence, and double disc zone spacing, will all affect overburden deformations and ruptures [48–52]. Therefore, overburden fractures are a complex nonhomogeneous and uncertain stochastic process, which are influenced by the dip angles of coal seams, mining disturbances, rock properties, and ground stress conditions, which in turn affect rock seam permeability [53–57]. The overturning instability damage mode of the rock mass was studied, and the stability was analyzed and predicted [58, 59]. The effects of uneven fracture distributions in the formation on permeability were studied [60, 61]. Adhikary and Guo [62], Guo et al. [63], Schatzel et al. [64], and Wang et al. [65] evaluated the permeability evolution of overburden disturbed by longwall mining and investigated the effect of fracture network geometry on permeability evolution. Meng et al. [49], Pan and Connell [66], and

(a) (b) (c)

Figure 2: Possible effects of strata fractures. (a) Underground coal fires; (b) groundwater influx; (c) gas decompression and extraction.

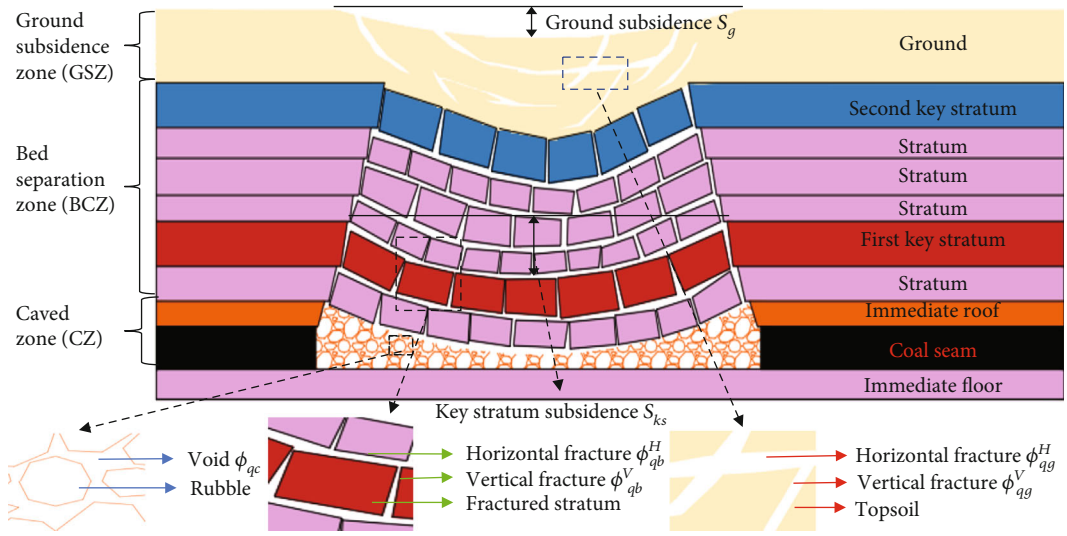

Figure 3: Diagram of overburden fracture and subsidence disturbed by horizontal coal seam mining.

Zhang and Shen [25] systematically studied the influence of rock damage on rock permeability during coal mining and established a coupled stress-permeability model. These studies have shown that fractures in overlying strata are characterized by an apparently nonhomogeneous and random distribution, but they were more concerned with the variations in permeability. However, research into void fraction, an important parameter influencing permeability, is lacking, and research into the randomly nonhomogeneous distribution characteristics of void fraction is even rarer.

In this paper, a three-dimensional distribution model for void fractions in each partition of the disturbed strata of inclined coal seam mining was established. Based on similar physical simulation experiments and digital image processing techniques, the random distribution characteristics of void fractions were obtained and the three-dimensional random distribution model for void fractions was constructed. The model was based on the key stratum theory and random medium theory and considered the gravity effects of the overlying strata and dip angle of the rock strata. The experimental results verified the accuracy of the theoretical results. The results show that the model is effective for calculating void fractions of disturbed rock strata in inclined coal seam mining and will provide theoretical guidance for safely mining inclined coal seams and coalbed methane.

2. Three-Dimensional Deterministic Distribution Model of Void Fractions

2.1. Three-Dimensional Model of Overburden Subsidence

2.1.1. Key Stratum Subsidence. Longwall mining is a common mining method for underground coal seam mining. During longwall seam mining, as the mining length increases, the overburden will be destabilized gradually, sink and subsequently collapse. The key stratum has an important influence on rock strata movement. Key stratum is present in most geological conditions, and the key stratum theory has been widely applied to analyze mining overburden movements. Based on the key stratum theory, the expression for key stratum movement in horizontal coal seam mining can be derived as [67–69]

$$Si(x,y) = \frac{S_{0i}\left\{1-\left[1+\exp\left((2lx-|2lx-4x|)/li-2\right)\right]^{-1}\right\}\cdot\left\{1-\left[1+\exp\left((2ly-4|y|)/li-2\right)\right]^{-1}\right\}}{1-\left[1+\exp\left(2ly/li-2\right)\right]^{-1}}, \quad (1)$$

where Si is the subsidence of the i^{th} key stratum in the x-y plane in the Cartesian coordinate system (m); $S_{0i} = M - \sum h_i(Kp_i - 1)$, where S_{0i} is the maximum subsidence amount of the i^{th} key stratum (m), M is the thickness of the coal seam (m), h_i is the distance between the i^{th} key stratum and the coal seam (m), and Kp_i is the bulking

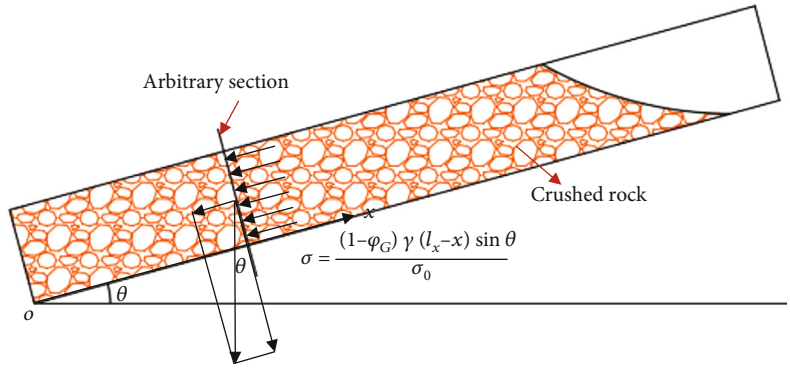

Figure 4: Diagram of a rock mass subjected to inclination and gravity.

factor of rock blocks between the i^{th} key stratum and the coal seam; $li = hi\sqrt{\sigma_{ti}/3q}$, where l_i, h_i, and σ_{ti} are the broken length (m), thickness (m), and tensile strength (MPa) of the i^{th} key stratum, respectively; q is the load on the i^{th} key stratum (MPa); and l_x and l_y are the dip length (m) and strike length (m) of the mined-out zone, respectively.

2.1.2. Ground Subsidence. The movements of individual rock masses or soil particles are complex when fracture and subsidence of the strata are triggered by coal seam mining, which in turn triggers surface movement. Due to this characteristic that influences the movement of geotechnical bodies, it is difficult to treat them as simple elastomers or elastoplastic bodies and to analyses the state of motion of individual geotechnical masses using classical mechanics. However, a large number of actual measurements have shown that a clear regularity exists in the general movement trend of the geotechnical body. In this case, better results can be obtained by applying probabilistic statistical methods. According to the theory of random media, the geotechnical body is considered a random medium. From a statistical perspective, the entire inclined coal seam can be decomposed into an infinite number of infinitely small excavation units. The impact from the entire excavation on the ground surface should be equal to the sum of the impacts from the many infinitely small excavation units that make up the excavation. The subsidence of the ground surface due to underground excavation can be expressed by the following equation [23]:

$$Sg(x,y) = \int_{-\infty}^{+\infty}\int_{-\infty}^{+\infty} \frac{Skm(\xi,\eta)}{H^2\cot^2\beta f} \cdot \exp\left\{-\frac{\pi}{H^2\cot^2\beta f}\left[(x-\xi)^2 + (y-\eta)^2\right]\right\} d\xi d\eta, \tag{2}$$

where $Sg(x,y)$ and $Skm(\xi,\eta)$ are the subsidence in the ξ-η coordinate plane for the horizontal coal seam mining surface and the main key stratum, respectively; H is the distance from the ground surface to the main key stratum (m); βf is the influence angle (°), which reflects the degree of influence from the settlement of the main key stratum on the surface; and the remaining cut $\cot\beta_f$ can be expressed as the ratio of the influence radius to the main key stratum depth.

2.2. Three-Dimensional Deterministic Distribution Model of Void Fractions. The disturbed overburden of coal seam mining can be divided into three zones: caved zone, bed separation zone, and ground subsidence zone. The caved zone is the part of the overburden where the overlying rock of the coal seam collapses completely after the coal is mined out. As the overburden gradually subsides with the inconsistent movement, the overlying strata are fractured and separated. The area where the fissures and separations occur in the overburden is called the bed separation zone. The area above the bed separation zone is called the ground subsidence zone.

2.2.1. Caved Zone. In the caved zone, due to the relatively high degree of fragmentation in the fractured rock masses, the random noncomplete contact accumulation of rock masses with granular forms can be regarded as forming isotropic voids, and the void fraction can be calculated by dividing the volume of the void by the total volume of the void and rock masses (Figure 3):

$$\varphi_c(x,y) = \begin{cases} \varphi_c^m + \varphi_c^0 = 1 - \dfrac{hd}{hd + M - S_1(x,y)} + \varphi_c^0, & x \in [0, lx], y \in \left[-\dfrac{ly}{2}, \dfrac{ly}{2}\right], \\ \varphi_c^0, & \text{others}, \end{cases} \tag{3}$$

where $\varphi_c(x,y)$ is the void fraction in the caved zone by horizontal seam mining; φ_c^m is the void fraction of mining-induced voids by horizontal seam mining; φ_c^0 is the initial void fraction of the immediate roof; $S1$ is the subsidence amount of the first key stratum that is nearest to the coal seam (m); hd is the immediate roof thickness (m); and M is the coal seam thickness (m).

A large number of field investigations have shown that the dip angle of the coal seam significantly influences the movement of the overlying rock strata and the distribution of void fraction. Below, the influence of the overlying rock strata dip angle and gravity was considered, and the void fraction influence factor affected by the dip angle and gravity was established. From this, the void fraction of the overburdened rock

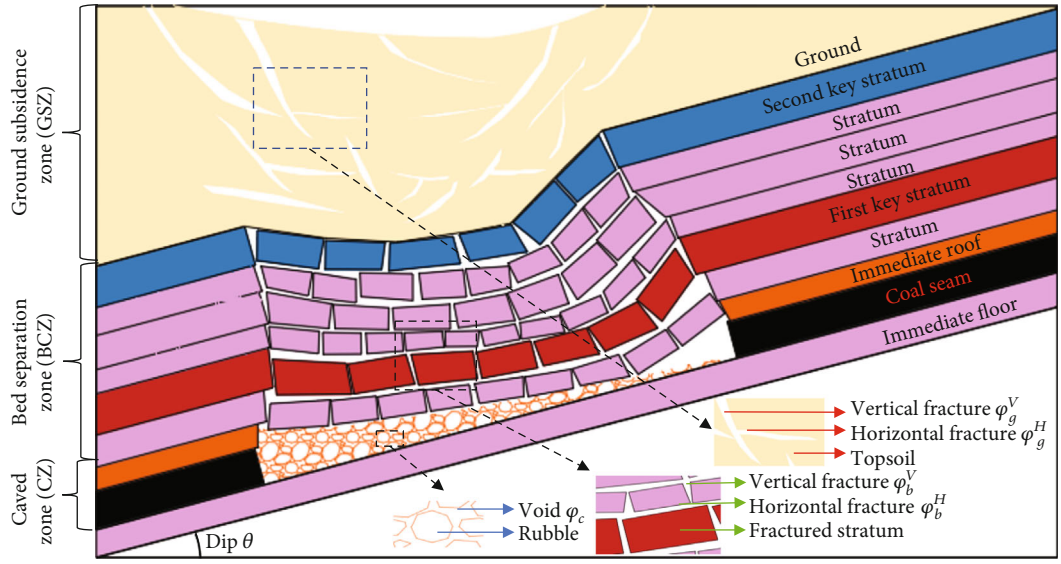

Figure 5: Diagram of overburden fracture and subsidence disturbed by inclined coal seam mining.

perturbed by inclined coal seam mining can be calculated from the corresponding void fraction of overburdened rock perturbed by horizontal coal seam mining.

The variation curve for the void fraction on the dip axis directions ($y = 0$) of the bottom plate of the mining-out zone can be expressed by the following equation [70]:

$$\varphi_{G(y=0)} = 1 - \frac{h_d}{h_d + H - w_{b(y=0)}}, \tag{4}$$

of these

$$w_{b(y=0)} = \left[H - h_d\left(K_{pb} - 1\right)\right]\left(1 - e^{-x/2l}\right), \tag{5}$$

where $\varphi_{G(y=0)}$ is the void fraction variation curve on the dip axis of the bottom slab in the mining area; h_d is the direct top thickness (m); H is the mining height or extraction and release height (m); $w_{b(y=0)}$ is the subsidence of the basic top distributed along the midaxis of the strike of the bottom slab of the mining area (m); K_{pb} is the residual fragmentation and swelling factor of the broken rock mass at the direct roof; and l is the length of the broken rock mass of the basic roof (m).

According to the theory of the "O" circle and field measurements, the void fraction in the working face inclination is larger in the hollow area near the end of the upper and lower lanes than in the middle of the hollow area. The variation coefficient of the void fraction deviating from the origin of the x-axis in the strike of the working face (x-axis direction) is in accordance with the following relationship [71]:

$$\varphi_{G,y} = 1 + e^{-0.15\left(\frac{l_y}{2} - |y|\right)} \tag{6}$$

From the analysis in Figure 4, the compressive stress at any interface on the inclination due to the effect of the loose rock's own gravity and the dip angle of the coal seam in the mining area is expressed as

$$\sigma = \frac{(1 - \varphi_G)\gamma(l_x - x)\sin\theta}{\sigma_0}, \tag{7}$$

where σ is the relative compressive stress in either section (MPa); θ is the coal seam dip (°); γ is the bulk weight of the fallen rock (N/m^3); σ_0 =1 (MPa); and under practical coal mine conditions, the bulk weight of a rock fall is typically 2×10^4 to 3×10^4 N/m^3.

When mining inclined coal seams, the void fraction of loose rocks in the mining area will be affected by the extrusion of rock gravity, the lower side of the mining area is subject to a large gravity load and high degree of compaction, and the void fraction is relatively small on the lower side, while the opposite is true on the upper side of the mining area. The polynomial regression equation of the variations in void fractions with axial stress in the broken rock masses can be expressed as [71]

$$\varphi_\gamma = \beta_3\sigma^3 + \beta_2\sigma^2 + \beta_1\sigma + \beta_0. \tag{8}$$

Since the compressive stress caused by the self-weight of the rock is affected by both rock voids and frictional forces, the quadratic and cubic terms in equation (8) can be neglected:

$$\varphi_G(x, y) = \beta_1\sigma + \varphi_{G,y=0} \cdot \varphi_{G,y}. \tag{9}$$

Substituting the parameters of each expression gives

$$\varphi_G(x, y) = \beta_1 \cdot \frac{(1 - \varphi_G)\gamma(l_x - x)\sin\theta}{\sigma_0} + \left[1 + e^{-0.15\left(\left(l_y/2\right) - |y|\right)}\right] \cdot \left\{1 - \frac{h_d}{h_d + H - \left[H - h_d\left(K_{P_b} - 1\right)\right]\left(1 - e^{-x/2l}\right)}\right\}. \tag{10}$$

Simplify to obtain

$$\varphi_G(x,y) = 1 - \frac{\left[1 + e^{-0.15\left(\left(l_y/2\right)-|y|\right)}\right] \cdot \left\{1 - \left(h_d/\left(h_d + H - \left[H - h_d\left(K_{P_b} - 1\right)\right]\left(1 - e^{-x/2l}\right)\right)\right)\right\} - 1}{\beta_1 \sigma_0^{-1} \gamma (l_x - x) \sin\theta + 1}. \tag{11}$$

The influence factor for the void fraction distribution is established as

$$\frac{\varphi_G(x,y)}{\varphi_c(x,y)} = G(x,y), \tag{12}$$

when the rock fall is shale, $\beta_1 = -0.0488$; when the rock fall is mudstone, $\beta_1 = -0.028$; and when the rock fall is sandstone, $\beta_1 = -0.0254$ [71].

From the influence of inclined seam mining inclinations and the gravity of the seam, the void fraction distribution of the inclined seam mining in the caved zone is shown as follows (Figure 5):

$$\varphi_{qc}(x,y) = G \cdot \varphi_c(x,y), \tag{13}$$

where $\varphi_{qc}(x,y)$ is the void fraction in the caved zone for inclined coal seam; G is the impact factor; and $\varphi_c(x,y)$ is the void fraction in the caved zone from horizontal seam mining.

2.2.2. Bed Separation Zone. The differential settlement of each rock stratum leads to interlaminar delamination between two adjacent rock strata, which in turn produces horizontal fractures. At the same time, the fractured rock masses rotate during settlement and move improperly against each other, producing vertical fractures. Therefore, the fractured rock masses in the bed separation zone can be regarded as a nonhomogeneous and anisotropic porous medium (Figure 3). According to the definition of void fraction, the void fraction of a horizontal fractures can be expressed as the ratio of the settlement difference to the spacing between adjacent rock layers, as shown in Equation (14). The void fraction of vertical fractures can be expressed as the ratio of the area increment after the formation settled to the total area, as shown in Equation (15).

$$\begin{aligned}\varphi^H_{b(i,i+1)}(x,y) &= \varphi^{HM}_{b(i,i+1)} + \varphi^0_b \\ &= \frac{Si(x,y) - Si+1(x,y)}{\sum hi + 1 - \sum hi + Si(x,y) - Si+1(x,y)} + \varphi^0_b,\end{aligned} \tag{14}$$

$$\begin{aligned}\varphi^V_{b(i)}(x,y) &= \varphi^{VM}_{b(i)} + \varphi^0_b \\ &= 1 - \frac{1}{\sqrt{1 + \left(\partial Si(x,y)/\partial x\right)^2 + \left(\partial Si(x,y)/\partial y\right)^2}} + \varphi^0_b.\end{aligned} \tag{15}$$

Combining the calculation methods of void fraction by horizontal coal seam mining and the influence from the inclination angle of the inclined coal seam and the gravity of the fractured rocks, similar to the caved zone, the influence factor for the void fraction distribution in the caved zone can be used as the influence factor in the bed separation zone. The void fraction from horizontal fractures and vertical fractures can be calculated by the equation below (Figure 5).

Table 2: Geometric properties of rock blocks in the similar simulation experiments.

Rock types	Thickness (cm)	Breaking length (cm)	Width (cm)
Sandy mudstone	2	2.5	3
Fine sandstone	3	4.2	3
Siltstone	5	6.7	3
Sandy mudstone	4	3.8	3
Gritstone	3	3.4	3
Sandy mudstone	3	4.5	3
Fine sandstone	2	1.9	3
Sandy mudstone	1	0.7	3
Coal seam	2	—	3

$$\varphi^H_{qb(i,i+1)}(x,y) = G \cdot \varphi^H_{b(i,i+1)}(x,y), \tag{16}$$

$$\varphi^V_{qb(i)}(x,y) = G \cdot \varphi^V_{b(i)}(x,y). \tag{17}$$

The total void fraction is the sum of the horizontal and vertical void fractions and can be obtained by adding the horizontal and vertical void fractions:

$$\varphi^T_{qb}(x,y) = \varphi^V_{qb(i)}(x,y) + \varphi^H_{qb(i,i+1)}(x,y), \tag{18}$$

where $\varphi^H_{qb(i,i+1)}$ and $\varphi^V_{qb(i)}$ are the void fractions of horizontal and vertical fractures from inclined coal seam mining, respectively; $\varphi^H_{b(i,i+1)}$ and $\varphi^{HM}_{b(i,i+1)}$ are the total and mining-induced void fractions of the horizontal fractures between the i^{th} and $(i+1)^{\text{th}}$ key stratum by horizontal seam mining, respectively; $\varphi^V_{b(i)}$ and $\varphi^{VM}_{b(i)}$ are the total and mining-induced void fractions of the vertical fractures in the i^{th} key stratum by horizontal seam mining, respectively; φ^0_b is the initial void fraction of the basic roof; and φ^T_{qb} is the total void fraction in the bed separation zone by inclined coal seam mining.

2.2.3. Ground Subsidence Zone. Due to discontinuous deformation of the topsoil stratum caused by the variabilities in settlement at different locations of the key stratum controlling the subsidence of the topsoil stratum, many horizontal fractures appear as a result of discontinuous soil media displaced in the vertical direction interlocking. In addition, the settlement topsoil expands in the horizontal direction and increases in volume, resulting in vertical fractures (Figure 3). Therefore, the disturbed ground surface that was mined can be considered a nonuniform and anisotropic porous medium. Similar to the derived equations for the void fractions of horizontal

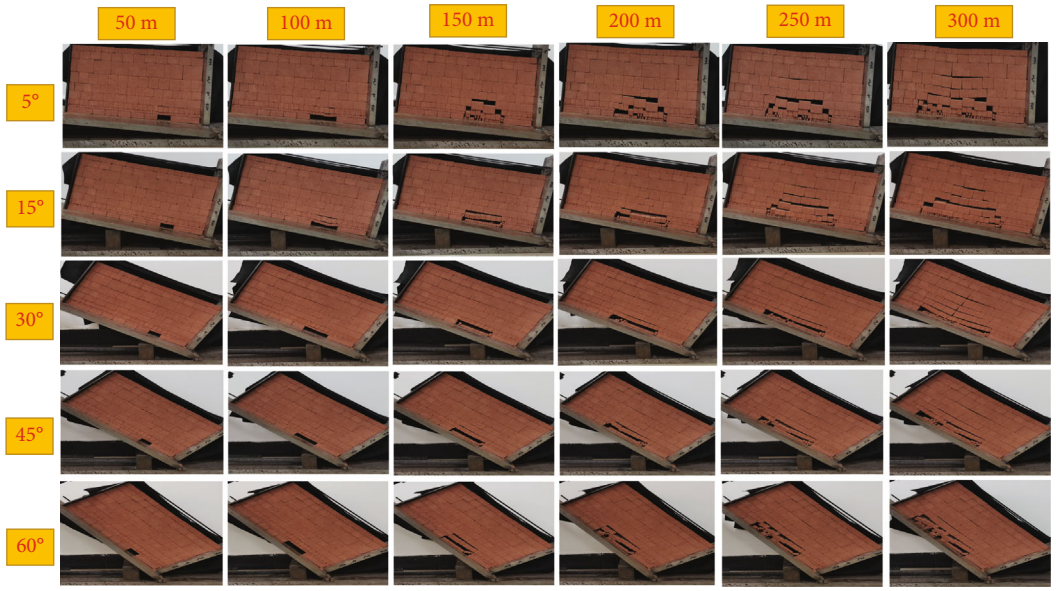

Figure 6: Collapse characteristics of disturbed overburdens during simulated mining of inclined coal seams at different dip angles and different excavation lengths.

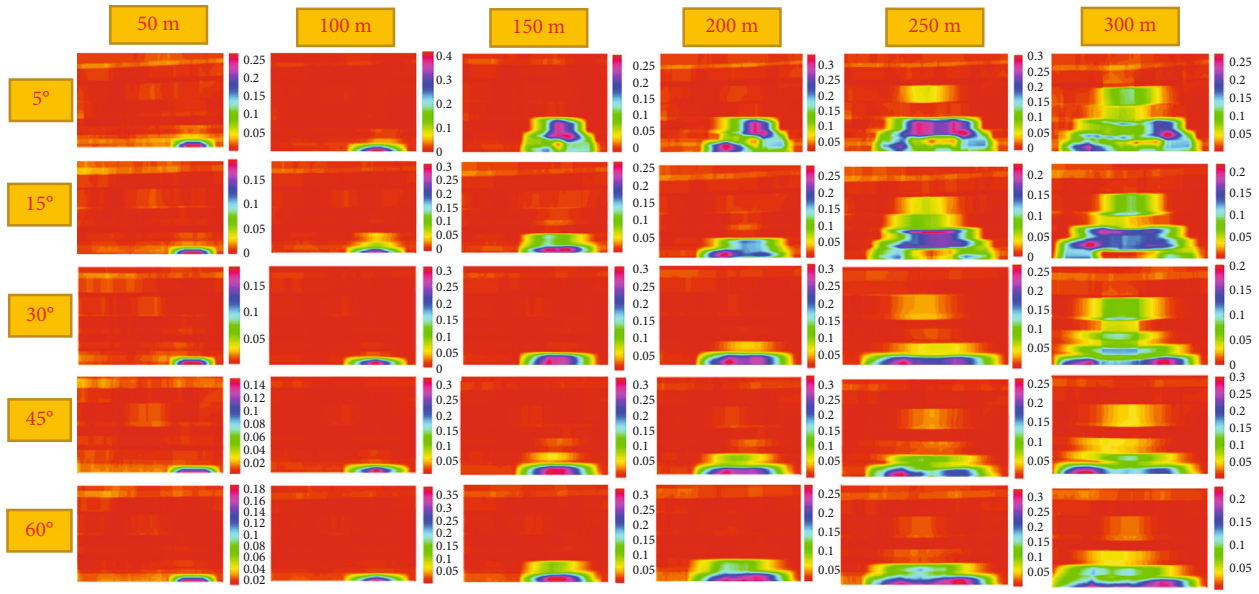

Figure 7: Cloud maps of the void fraction distributions of overburden images after coal seam excavations at different dip angles and different excavation lengths.

and vertical fractures in the bed separation zone, the void fractions of horizontal and vertical fissures in the ground subsidence zone can be expressed as

$$\varphi_g^H(x,y) = \varphi_g^{HM} + \varphi_g^0 = \frac{Skm(x,y) - Sg(x,y)}{H + Skm(x,y) - Sg(x,y)} + \varphi_g^0,$$

$$\varphi_g^V(x,y) = \varphi_g^{VM} + \varphi_g^0 = 1 - \frac{1}{\sqrt{1 + 0(\partial Sg(x,y)/\partial x)^2 + (\partial Sg(x,y)/\partial y)^2}} + \varphi_g^0. \quad (19)$$

Introducing the effect of the inclination from the inclined coal seam and the gravity of the fractured rocks, the horizontal and vertical void fractions in the ground subsidence zone can be calculated by the following equation (Figure 5):

$$\varphi_{qg}^H(x,y) = G \cdot \varphi_g^H(x,y), \quad (20)$$

$$\varphi_{qg}^V(x,y) = G \cdot \varphi_g^V(x,y), \quad (21)$$

where φ_{qg}^H and φ_{qg}^V are the void fractions of the horizontal and vertical fissures in the ground subsidence zone by inclined coal seam mining, respectively; φ_g^H and φ_g^V are the void fractions of

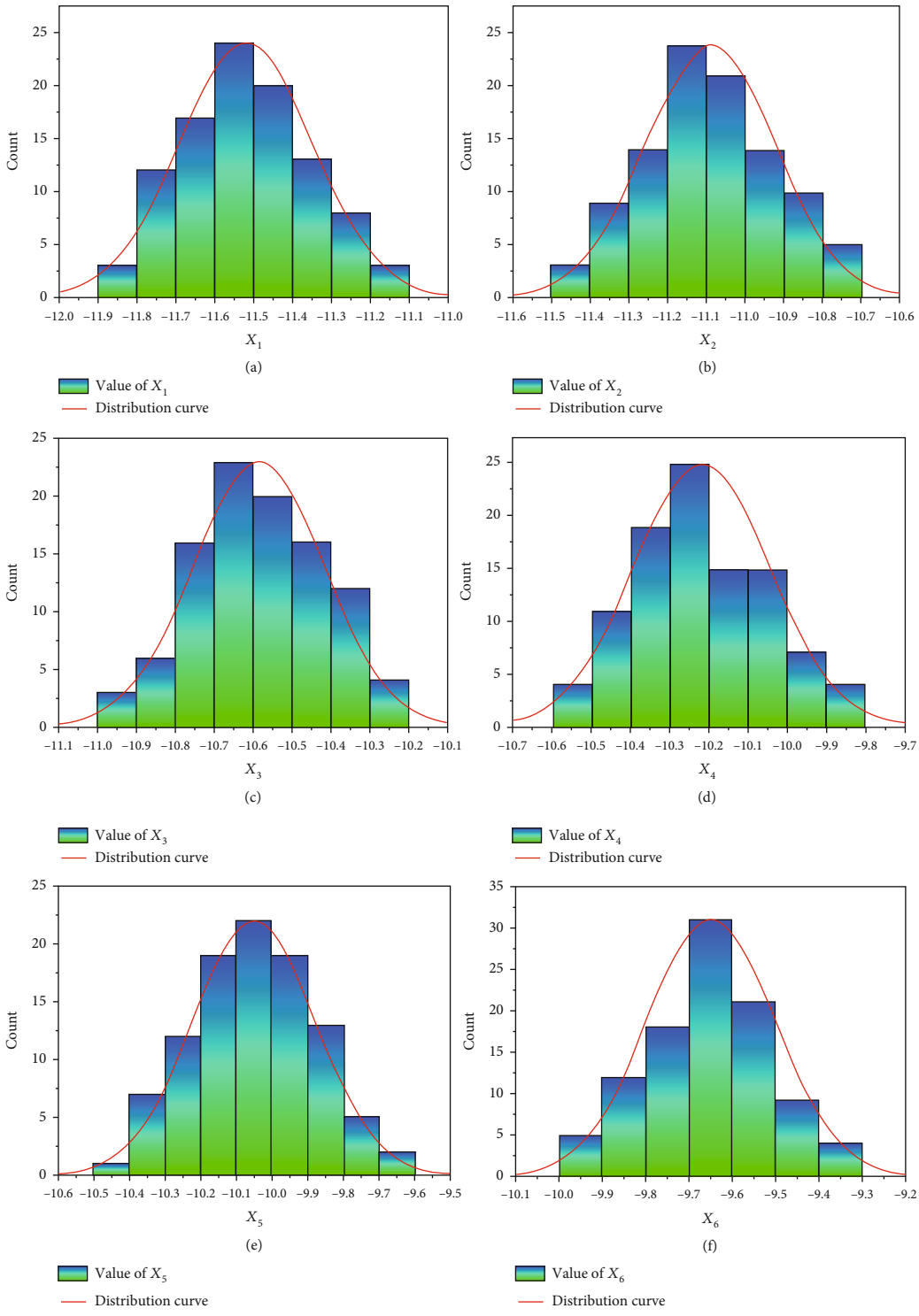

FIGURE 8: Statistical distribution of random variables constructed from void fractions under physical simulation tests at mining lengths of (a) 50 m, (b) 100 m, (c) 150 m, (d) 200 m, (e) 250 m, and (f) 300 m.

the horizontal and vertical fissures in the ground subsidence zone by horizontal seam mining, respectively; φ_g^{HM} and φ_g^{VM} are the void fractions of the mining-induced horizontal and vertical fissures in the ground subsidence zone by horizontal seam mining, respectively; and φ_g^0 is the initial void fraction of the topsoil layers.

3. Randomized Trial of Void Fraction Distribution

3.1. Experiment Approach. To realistically and objectively simulate the movement of the overlying rock disturbed by mining inclined coal seams, a similar simulation experiment with a geometric ratio of 1 : 1000 was conducted. In the

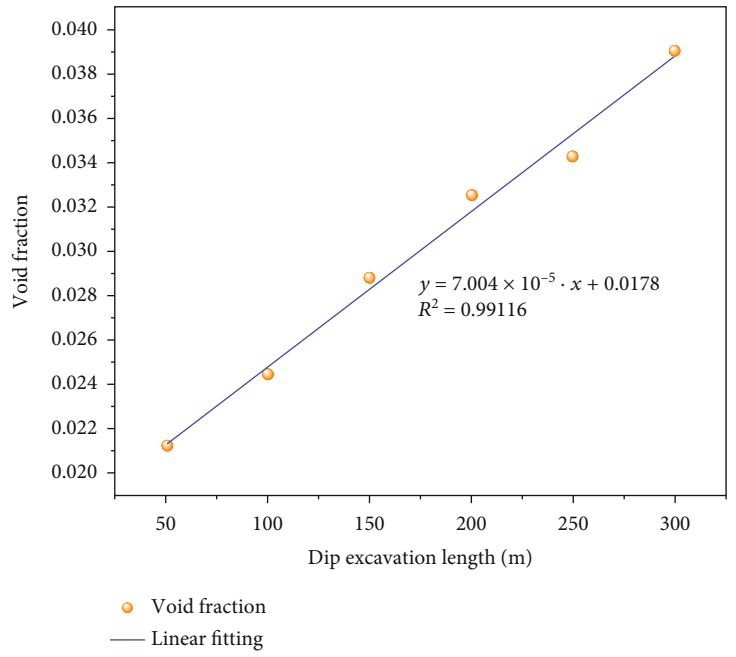

Figure 9: Average void fraction values for different mining lengths.

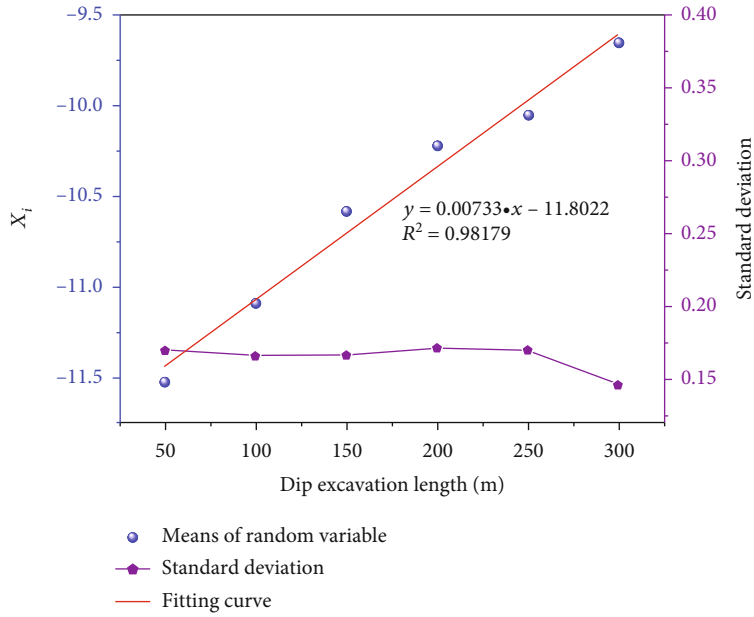

Figure 10: Means and standard deviations of random variables at different mining lengths.

similar simulation experiment, the geometric parameters of each rock layer are shown in Table 2.

In this similar simulation experiment, coal seam excavations with inclination angles of 5°, 15°, 30°, 45°, and 60° were simulated. In the process of excavation, the overlying rock strata are disturbed by the excavation and their equilibrium state are broken, and the rock strata develop towards a new equilibrium state in the area. The overlying rock strata are disturbed by the excavation and are broken in their equilibrium state. Once the overlying strata formation had moved and stabilized, photographs of similar simulated experimental rock formations were taken. Images of the overburdened rock after simulating coal seam excavations at 50 m, 100 m, 150 m, 200 m, 250 m, and 300 m in length are shown in Figure 6.

3.2. Digital Image Processing. The experimental photographs were binarized by selecting the appropriate grey scale values as thresholds based on the light intensity to distinguish the voids between rock masses. Then, the pixels of rock mass and void from the binarized images were extracted. The void fraction in the image is then obtained by dividing the total

number of void pixel by the total number of pixels of rock mass, according to the void fraction calculation methods. Based on the geometry of similar simulated physical rock strata combined with a similar geometric ratio, a traversal window of 300 × 150 pixels was constructed, and the whole image was traversed pixel by pixel to obtain a two-dimensional cloud map of the void fraction distribution, shown in Figure 7.

3.3. Experimental Results. Based on the Kozeny-Carman relationship between the permeability and void fraction of a loose medium and the results of Hoek and Bray's study of the Kozeny-Carman relationship, as shown in

$$k = \frac{\varphi 3}{(1-\varphi)2} . (Fs2s2Sg2) = \frac{k0}{0.241} \cdot \frac{\varphi 3}{(1-\varphi)2}, \quad (22)$$

the variable is logarithmically treated to construct the random variable X_i expressed as

$$Xi = \ln \left[\frac{\varphi i 3}{(1-\varphi i)2} \right] = 3 \ln \varphi i - 2 \ln (1-\varphi i), \quad (23)$$

where k is the permeability; φ is the void fraction; F_s is the shape coefficient; s is tortuosity; S_g is the surface area of the particles contained in the medium per unit mass; k_0 is the baseline permeability, which can be $10^3\,\mu m^2$; X_i is the random variable obtained by processing the test data of group i; and φ_i is the void fraction of rock block obtained from test group i.

The values of the random variables under the same mining length conditions were statistically analyzed to obtain the distributions of the random variable X_i, as shown in Figure 8. From Figure 8, it can be seen that the random variable X_i obeys normal distribution, where the random variables in the cases of excavation lengths of 50 m, 100 m, 150 m, 200 m, 250 m, and 300 m obey normal distributions $N_1 \sim (-11.5197, 0.02884)$, $N_2 \sim (-11.0894, 0.02766)$, $N_3 \sim (-10.5861, 0.02785)$, $N_4 \sim (-10.2189, 0.02946)$, $N_5 \sim (-10.0507, 0.0290)$, and $N_6 \sim (-9.6505, 0.0214)$. The values of void fractions for the six mining lengths were fitted as shown in Figure 9. The values of the random variables constructed from the void fraction of the six mining lengths along with their fit function and the standard deviations are shown in Figure 10.

4. Three-Dimensional Stochastic Distribution Model of Void Fractions

In the process of longwall mining of inclined coal seams, the subsidence of rock strata are non-homogeneous and dynamically random, due to the nonhomogeneity of the physical and mechanical properties of the rock strata and the influence of the dip angle. Therefore, the actual void fraction at each point of the overburden is a value that fluctuates around a certain range above and below the void fraction value from the theoretically determined model. From the calculation methods of void fraction and permeability, the random variables associated with void fractions were constructed and analyzed by several experimental statistical treatments to obtain the random variation law of the random variables, which were introduced into the deterministic model of void fractions to characterize the random distribution of void fractions in disturbed overburdens. It gives the model the advantage of combining theoretical calculations with actual conditions and improving model applicability and accuracy.

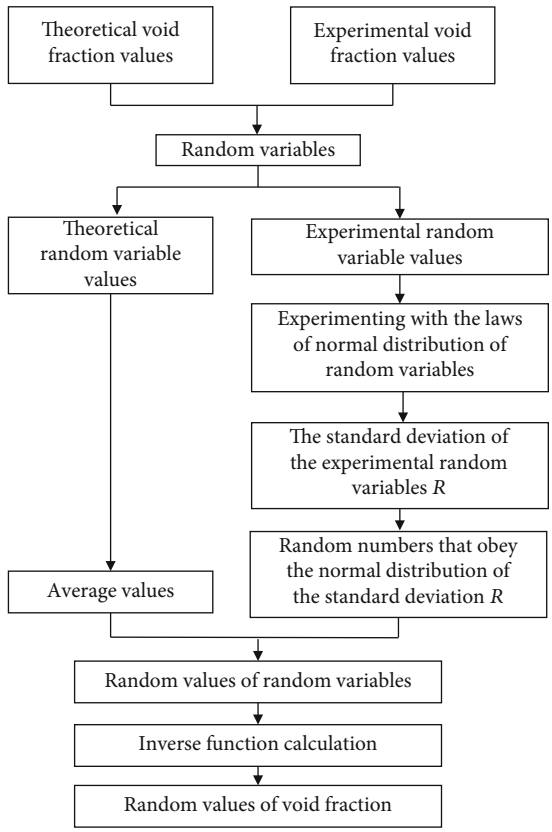

Figure 11: The process to obtain a stochastic distribution of void fractions.

First, the values of the void fraction at each point of the overburden rock calculated in the proposed void fraction theory are determined from the model as the mean values of the random model for void fractions at that point. And then the standard deviations of the constructed random variables associated with the void fraction were statistically analyzed by several experiments as the random characteristics of the void fraction at each point of the random model for void fractions. Applying this method to each point of the overburden, a three-dimensional stochastic discrete distribution model for the void fractions of the overburdens disturbed by longwall mining of inclined coal seam was obtained. The establishment process is shown in Figure 11.

Because the constructed random variable obeys the law of normal distribution, the random values of the random variables at each point corresponding to the extraction area can be expressed as

$$X_q^s(x,y) = X_q^d(x,y) + R \cdot \mathrm{randn}(x,y). \quad (24)$$

Table 3: Geometric properties and mechanical parameters of various rock strata overlying the coal seam.

ID	Rock types	Thickness (m)	Breaking Length (m)	Inclination (°)	Bulk density (KN/m^3)	Elastic modulus (10^4MPa)	Poisson's ratio	Tensile strength (MPa)	Cohesion (MPa)	Friction angle (°)
1	Sandy mudstone	20	25	30	24.28	0.89	0.17	2.07	6.89	35.9
2	Fine sandstone	30	42	30	24.12	2.48	0.21	3.06	5.77	38.8
3	Siltstone	50	67	30	24.17	1.27	0.23	3.57	6.66	38.5
4	Sandy mudstone	40	38	30	24.28	0.89	0.17	2.07	6.89	35.9
5	Gritstone	30	34	30	23.57	1.59	0.23	3.13	4.42	42.0
6	Sandy mudstone	30	45	30	23.57	0.78	0.15	1.09	11.00	32.1
7	Fine sandstone	20	19	30	23.95	1.74	0.14	2.62	7.27	38.8
8	Sandy mudstone	10	7	30	24.31	0.74	0.15	1.60	7.60	35.4

Note: ID 6 is the first key stratum; ID 3 is the second key stratum.

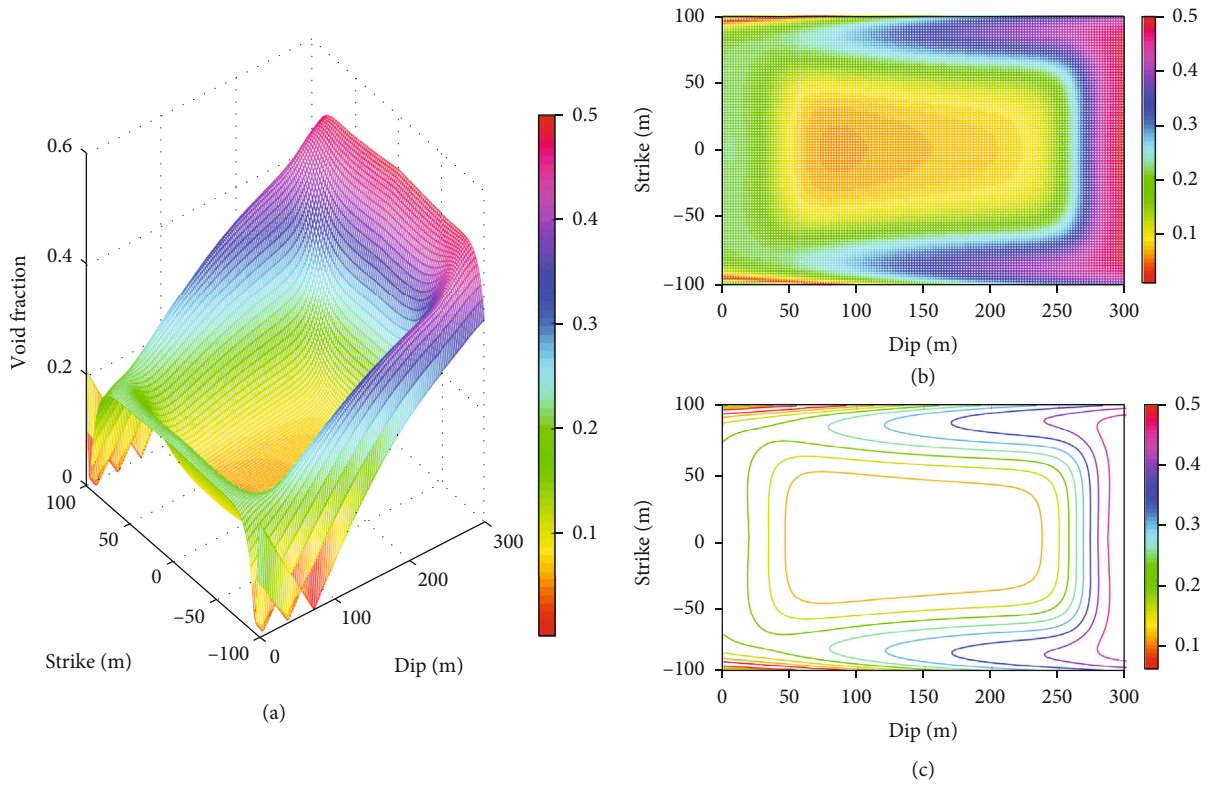

Figure 12: Void fraction distribution in the caved zone, including (a) curved-surface diagram, (b) distribution nephogram in the strike-dip plane, and (c) contour plots.

The relationship between the constructed random variables and the void fraction is defined as a function $F(x)$:

$$X_i = 3 \ln \varphi_i - 2 \ln \varphi_i = F(\varphi_i). \tag{25}$$

By calculating the inverse function of the function $F(x)$, the stochastic distribution characteristics of the void fraction of disturbed rock strata by longwall mining can be obtained:

$$\varphi_q^s = F^{-1}\left(X_q^s\right), \tag{26}$$

where $X_q^s(x, y)$ is the stochastic value; $X_q^d(x, y)$ is the theoretical calculated value; R is the standard deviation of X_i; randn(x, y) is the random numbers that obey the standard normal distribution; and φ_q^s is the stochastic void fraction.

5. Case Study

A longwall mining ground with an inclined coal seam was studied as an example. The inclination of the coal seam averaged 30°, the inclined length was 300 m, the strike width was 200 m, and the average thickness of the coal seam was 20 m. The geometrical characteristics and mechanical parameters of the rock strata overlying the coal seam are shown in Table 3.

5.1. Deterministic Distribution of Void Fractions. Using the derived Equations (13), (16), (17), (18), (20), and (21), the three-dimensional distribution of void fractions in the overburdens of caved zones, bed separation zones, and ground subsidence zones disturbed by inclined coal seam mining can be obtained.

5.1.1. Caved Zone. As can be seen in Figure 12, the void fraction in the caved zone is distributed in a "dustpan" shape in the xy-plane. The void fraction is largest around the upper end of the mining-out zone in the direction of the inclination (maximum value of 0.5002), but small near the central area (minimum value of 0.00081). The void fraction tends to decrease from the upper to the lower end of the zone in the direction of the inclination. The void fraction decreases sharply from the perimeter of the mined-out zone to the central area and then decreases slowly. This indicates that the voids in the cave zones are primarily concentrated around the perimeter of the mining-out zone, and the upper periphery is larger than the lower periphery in the inclination direction. In these areas, groundwater, methane, oxygen, and fumes are easily enriched.

5.1.2. Bed Separation Zone. In the bed separation zone, the distribution of horizontal void fraction in the xy-plane is shown in Figure 13. In the dip direction, the overburden horizontal void fraction resembles a double hump distribution with one high and one low. From the upper end to the lower end, the void increases first to the maximum peak and then decreases. Near the lower end of the dip, it increases to another peak and then gradually decreases.

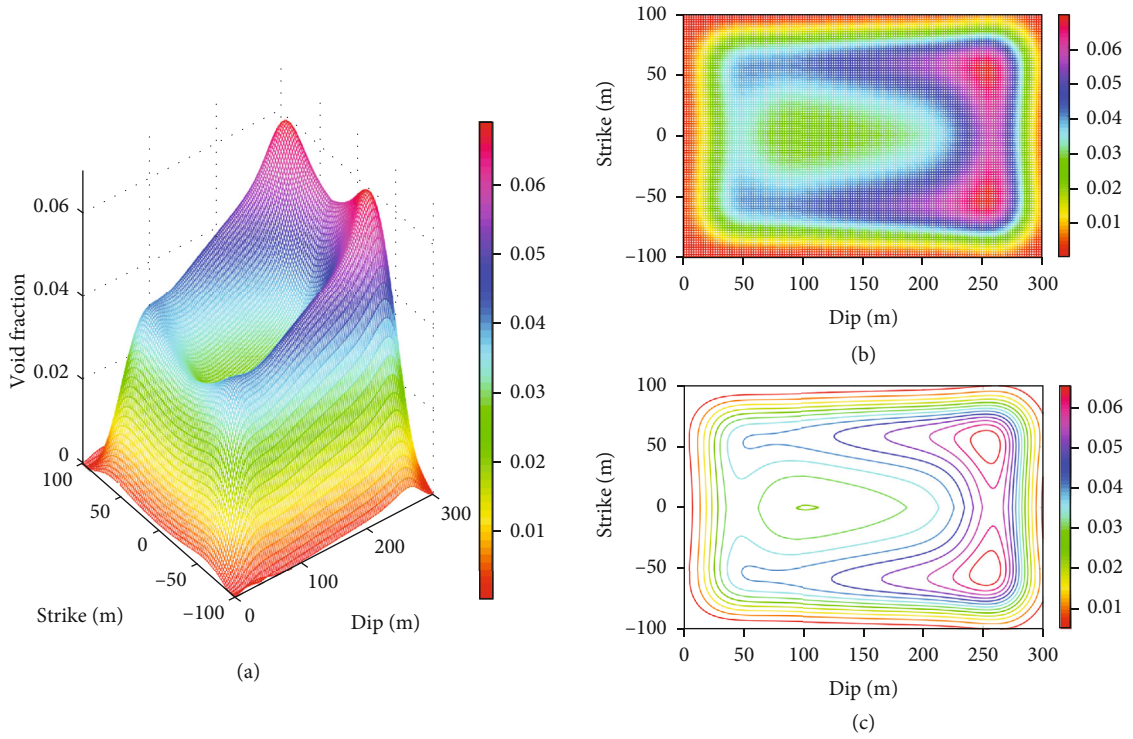

FIGURE 13: Horizontal void fraction distribution in the bed separation zone, including (a) curved-surface diagram, (b) distribution nephogram in the strike-dip plane, and (c) contour plots.

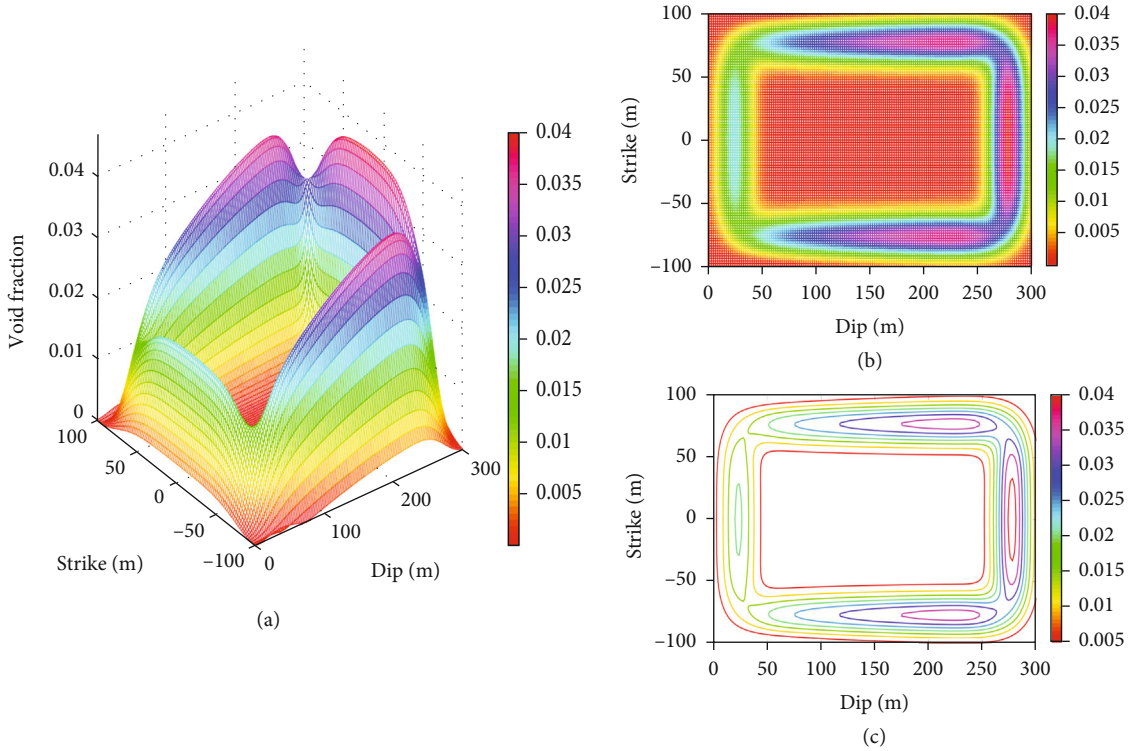

FIGURE 14: Vertical void fraction distribution in the bed separation zone, including (a) curved-surface diagram, (b) distribution nephogram in the strike-dip plane, and (c) contour plots.

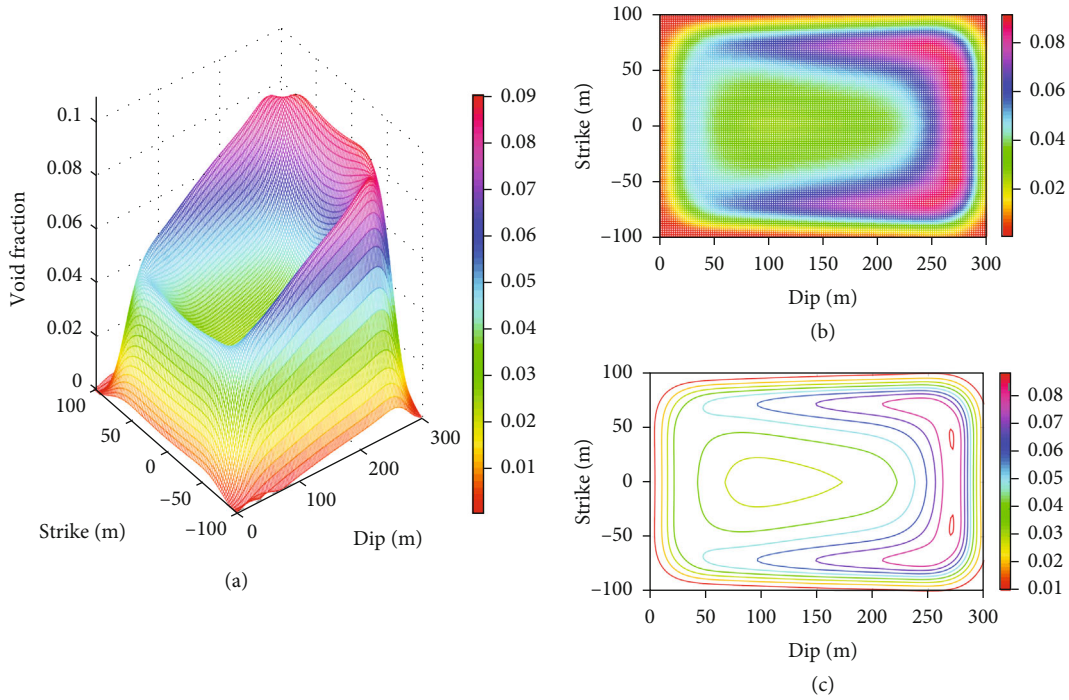

Figure 15: Total void fraction distribution in the bed separation zone, including (a) curved-surface diagram, (b) distribution nephogram in the strike-dip plane, and (c) contour plots.

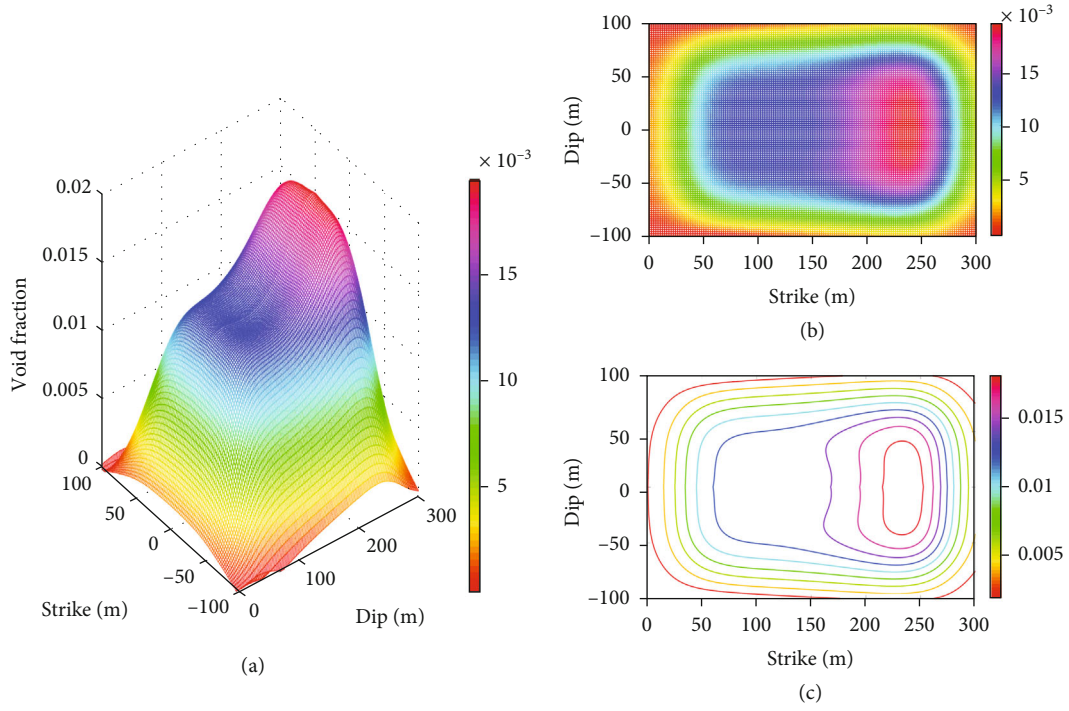

Figure 16: Transverse void fraction distribution in the ground subsidence zone, including (a) curved-surface diagram, (b) distribution nephogram in the strike-dip plane, and (c) contour plots.

The maximum value of the horizontal void fraction occurs at the upper end and then stabilizes in the central region near the lower end. The peak and trough values of the void fractions are greater at the upper end than at the lower end. In the strike direction, there is a symmetrical "M" shaped distribution, with both the peak and trough of the "M" shape

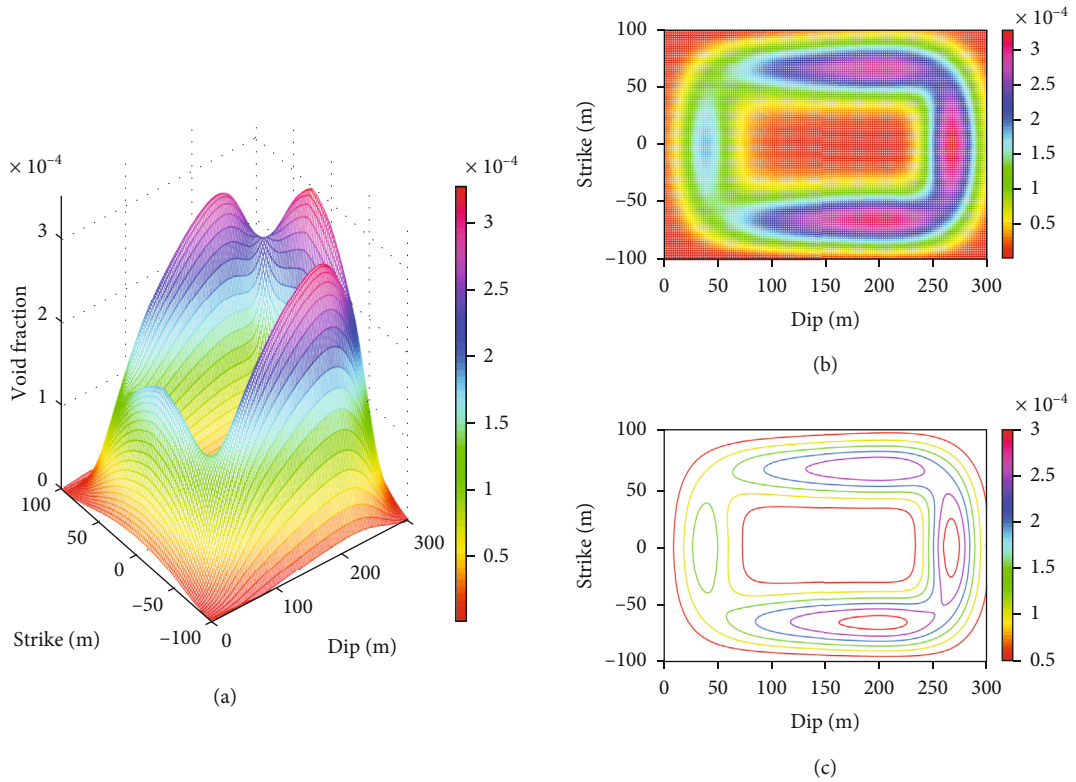

Figure 17: Longitudinal void fraction distribution in the ground subsidence zone, including (a) curved-surface diagram, (b) distribution nephogram in the strike-dip plane, and (c) contour plots.

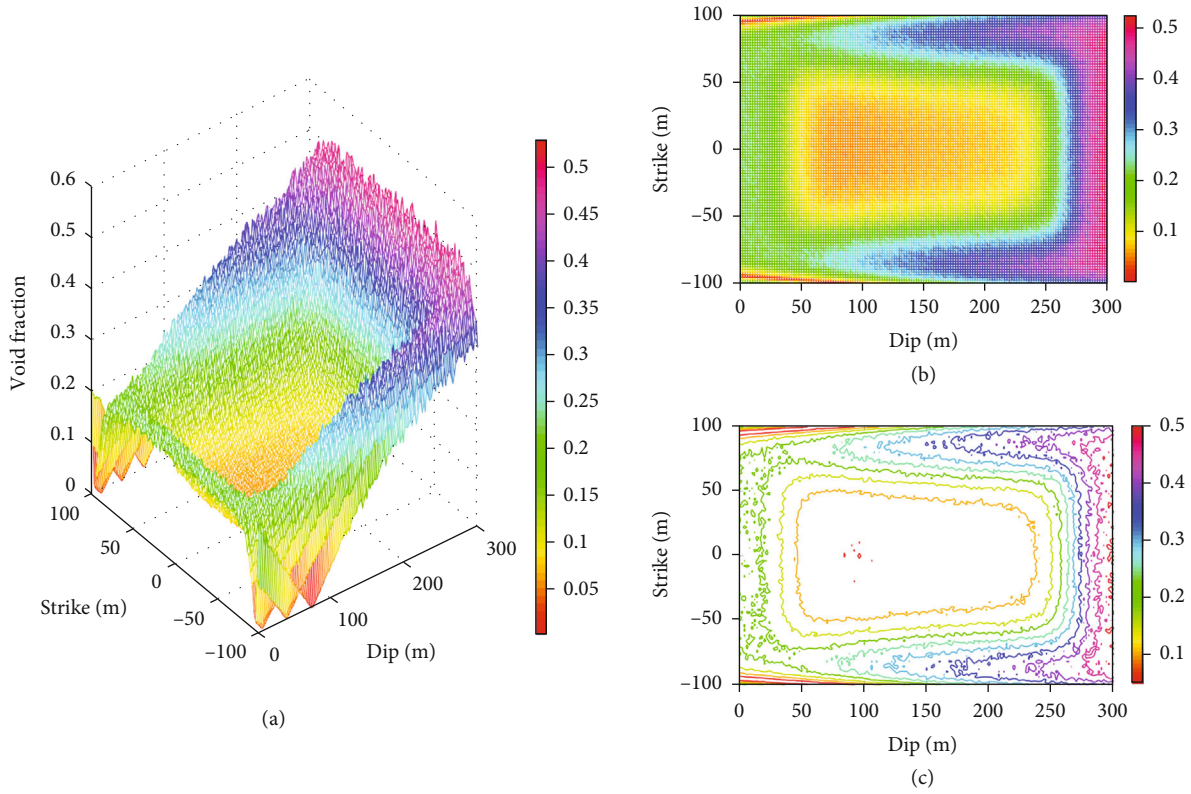

Figure 18: Stochastic distribution of void fractions in the cave zone, including (a) curved-surface diagram, (b) distribution nephogram in the strike-dip plane, and (c) contour plots.

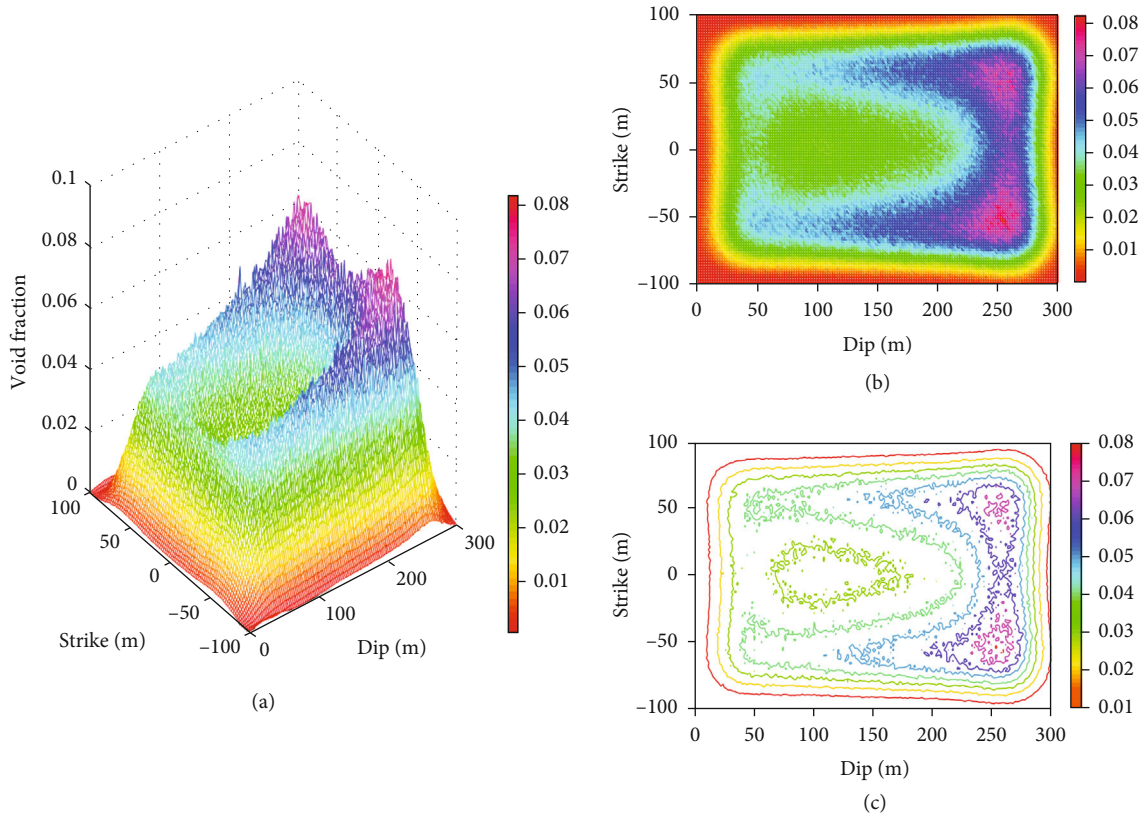

Figure 19: Stochastic distribution of horizontal void fractions in the bed separation zone, including (a) curved-surface diagram, (b) distribution nephogram in the strike-dip plane, and (c) contour plots.

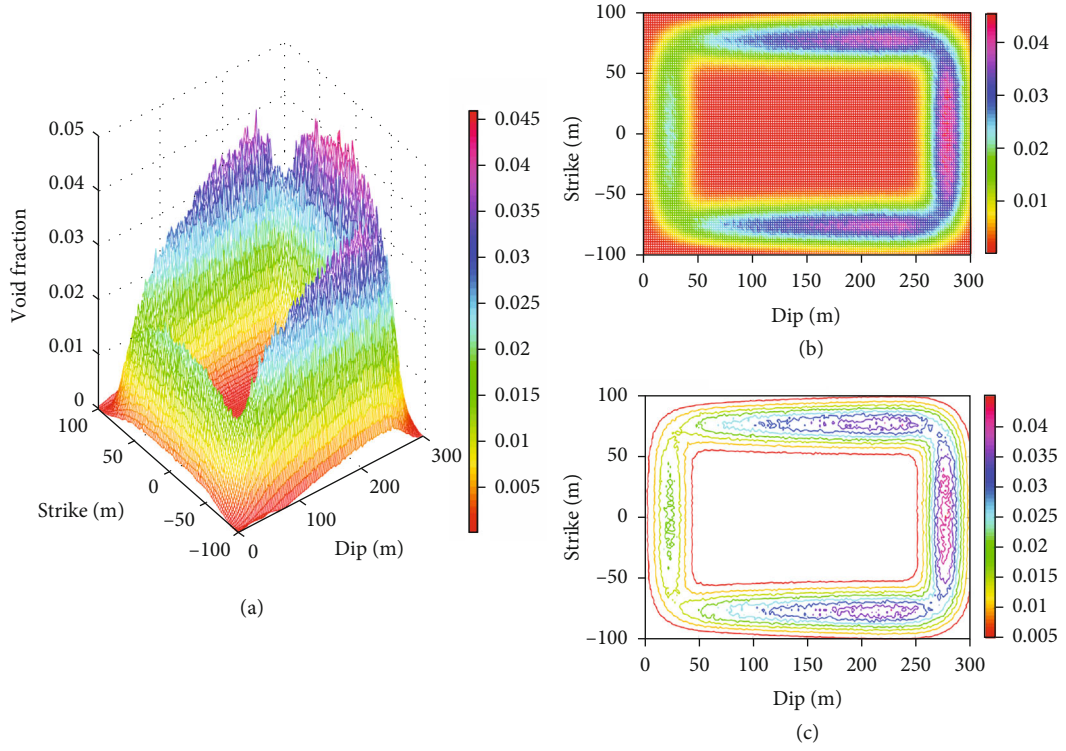

Figure 20: Stochastic distribution of vertical void fractions in the bed separation zone, including (a) curved-surface diagram, (b) distribution nephogram in the strike-dip plane, and (c) contour plots.

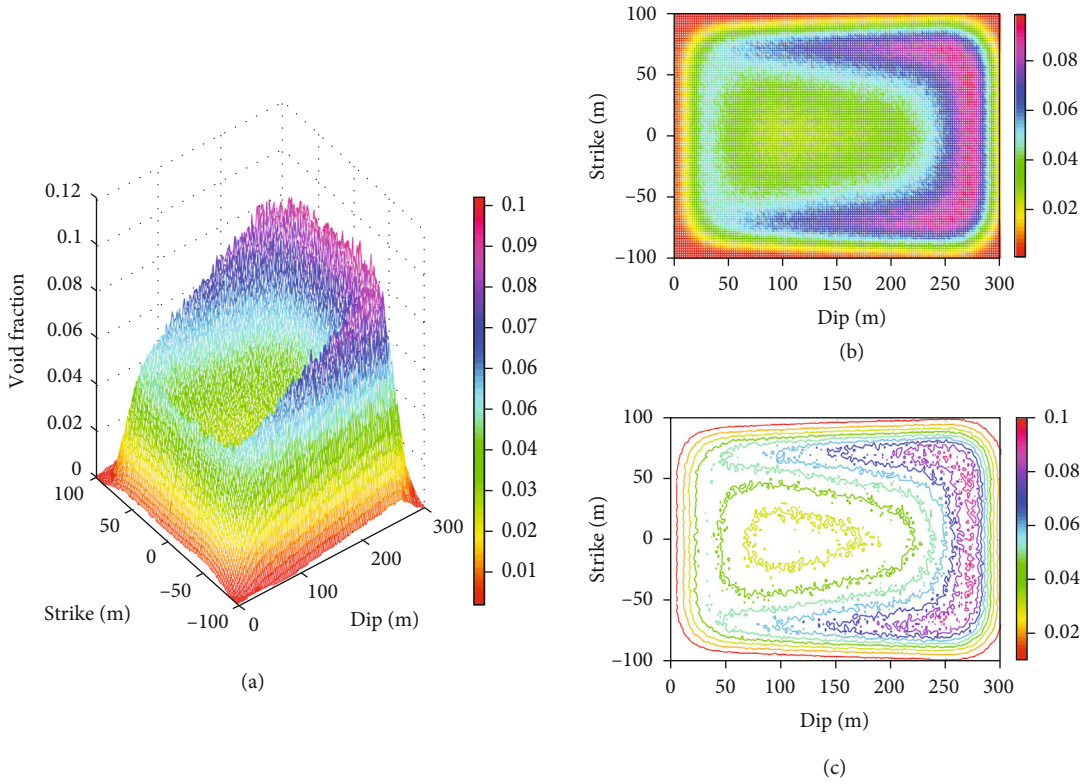

FIGURE 21: Stochastic distribution of total void fractions in the bed separation zone, including (a) curved-surface diagram, (b) distribution nephogram in the strike-dip plane, and (c) contour plots.

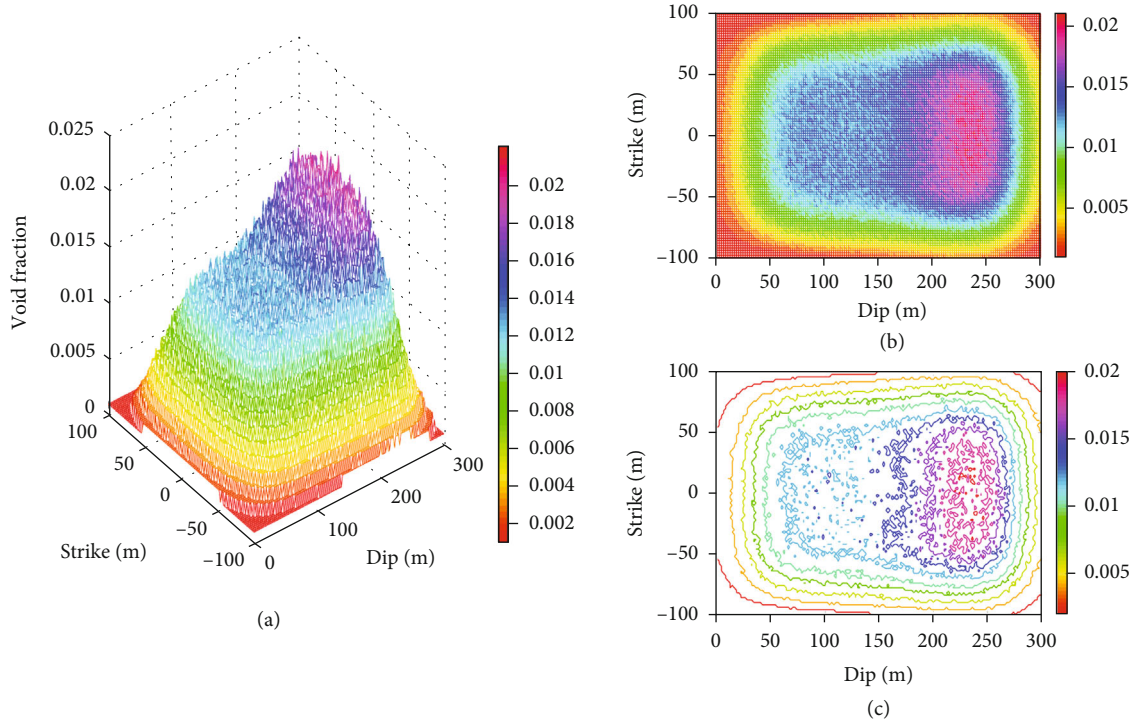

FIGURE 22: Stochastic distribution of transverse void fractions in the ground subsidence zone, including (a) curved-surface diagram, (b) distribution nephogram in the strike-dip plane, and (c) contour plots.

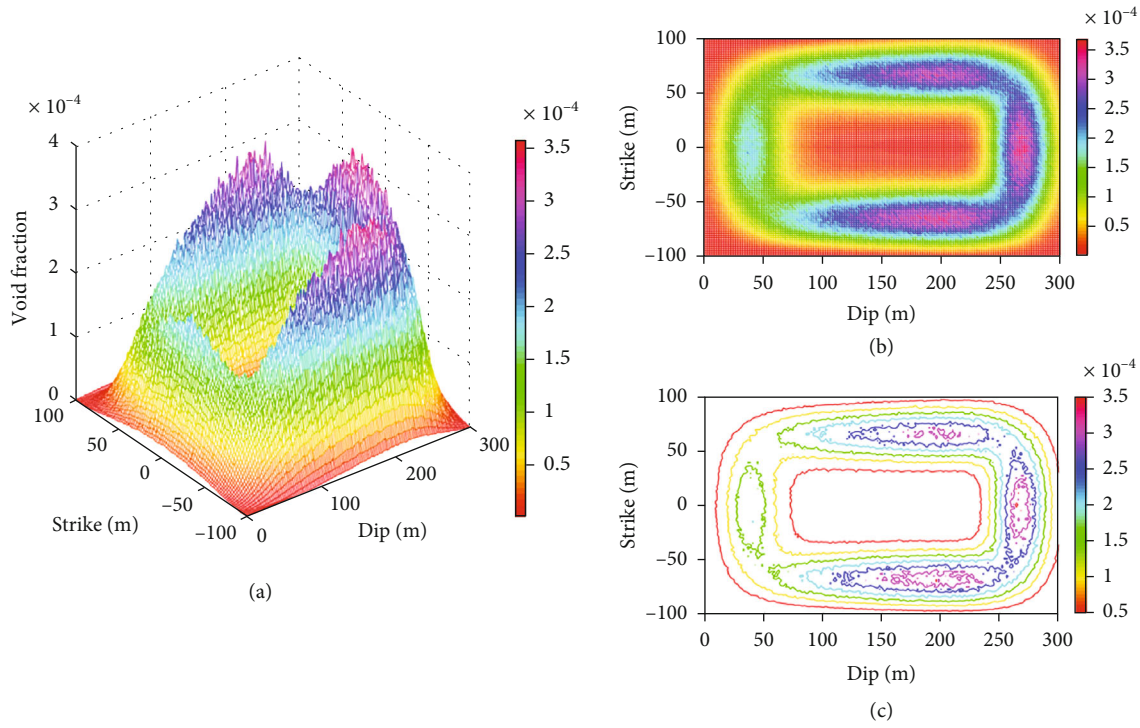

FIGURE 23: Stochastic distribution of longitudinal void fractions in the ground subsidence zone, including (a) curved-surface diagram, (b) distribution nephogram in the strike-dip plane, and (c) contour plots.

decreasing from the perimeter of the mined-out zone towards the central direction.

From Figure 14, it can be seen that the distribution of vertical void fractions in the *xy*-plane shows two nested basins having a high and low side, with different sizes and opening directions. In the dip direction, the vertical void fraction shows an inverted "U" shaped distribution around the perimeter of the mined-out zone, while in the middle, it is a double hump distribution with one high and one low. From the upper end to the lower end, the vertical void fraction increases rapidly and then decreases gradually at a certain rate around the mined-out area, decreasing rapidly near the lower end. In the area near the middle of the mined-out zone, the void fraction first increases rapidly to a maximum value, then decreases rapidly to a minimum value and trends towards a minimum value within a certain range in the middle, and then increases rapidly to another peak followed by a rapid decrease at the lower end. In the strike direction, the vertical void fraction has an inverted "U" shaped distribution around the mining area and an "M" shaped distribution in the central area, both of which are symmetrical in character. The peak and trough values of the "M" shaped distribution show a decreasing trend from the upper to the lower end. The four corners of the rectangular area corresponding to the mined-out zone exhibit a concave shape.

As can be seen in Figure 15, the distribution of total void fractions shows a double hump distribution with one high and one low in the dip direction and an "M" shaped distribution in the strike direction. Compared to the shape of the horizontal and vertical void fraction distribution, the crests and troughs of the total void fraction distribution have been significantly reduced.

5.1.3. Ground Subsidence Zone. In the ground subsidence zone, the horizontal void fraction shows an inverted basin-shaped distribution with a sloping base, as shown in Figure 16. In the dip direction, the distribution is an inverted "U" shaped with a sloping bottom, and in the strike direction it shows an inverted "U" shaped distribution. The shape of the vertical void fraction distribution is similar to that of the vertical void fraction distribution in the bed separation zone, as shown in Figure 17. Both the horizontal and vertical void fraction are smaller than the void fraction in the bed separation zone, due to the gradual decrease in mining disturbances from deep underground to the surface.

5.2. Stochastic Distribution of Void Fractions. For the three-dimensional distribution model for void fraction, the obtained void fraction is taken as the expected value, and the variance of the random variables obeying a normal distribution obtained from the statistical analysis of similar physical simulation experiments are taken as the stochastic nature of the void fraction. Figures 18–23 show the random distributions of void fractions in the cave zone, bed separation zone, and ground subsidence zone. The overall trend of the random distribution of void fraction is consistent with that shown by the deterministic model for void fractions. The values of the stochastic void fraction are values that

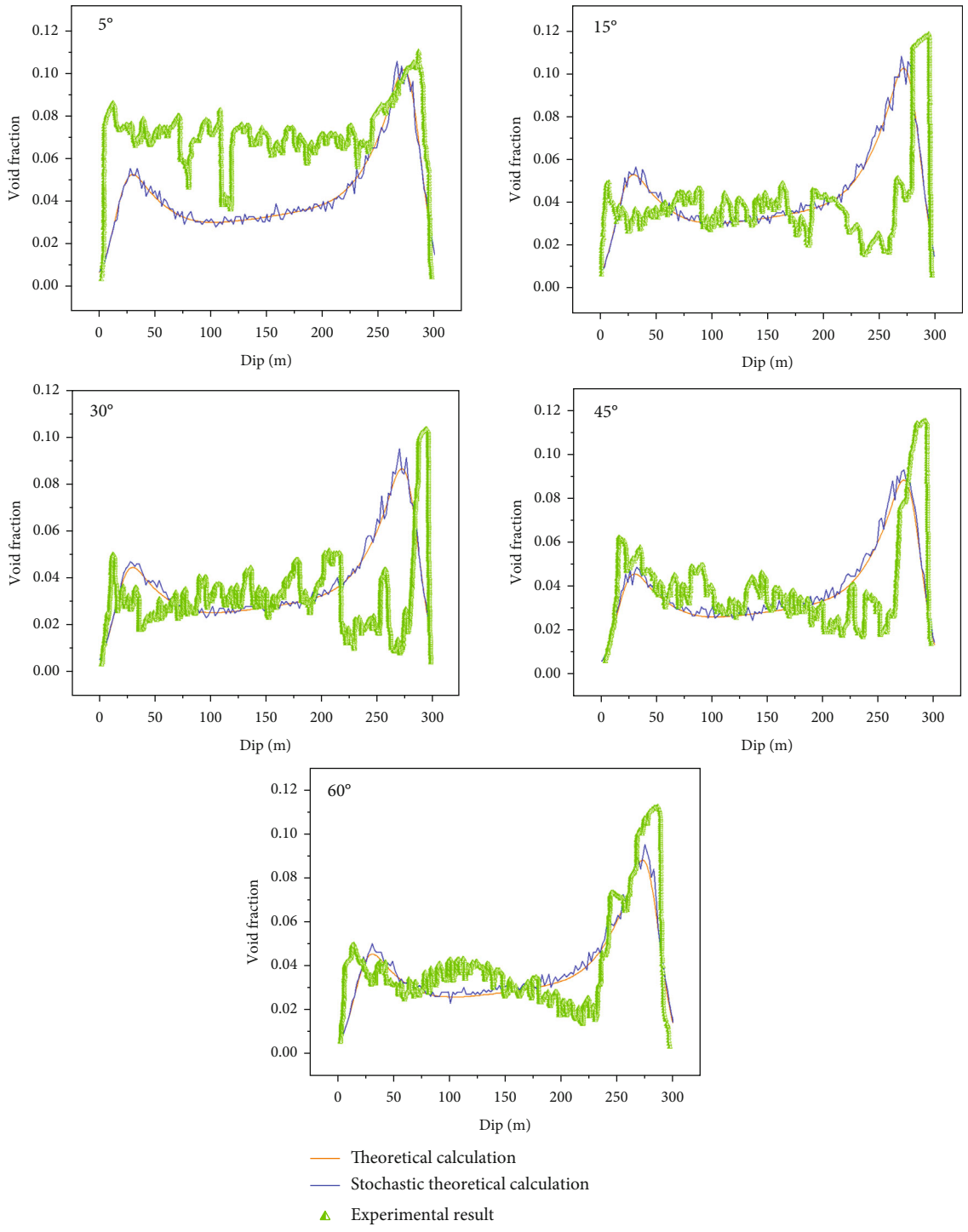

Figure 24: Comparison of void fractions for different inclination angles, including theoretical calculations, stochastic calculations, and experimental results.

fluctuate around a range of the theoretical values, which are more reflective of the actual nonhomogeneous dynamics that are featured in the field.

6. Discussion

6.1. Void Fractions for Different Inclination Angles. The experimental results for the total void fraction of the bed separation zone were compared with theoretical calculations and stochastic calculations. Overall, the results from the comparison show that the characteristics of the void fraction distribution in the bed separation zone at different inclination angles are basically among theoretical, stochastic, and experimental results, as shown in Figure 24. The experimental results also confirm the accuracies of the theoretical and stochastic calculations.

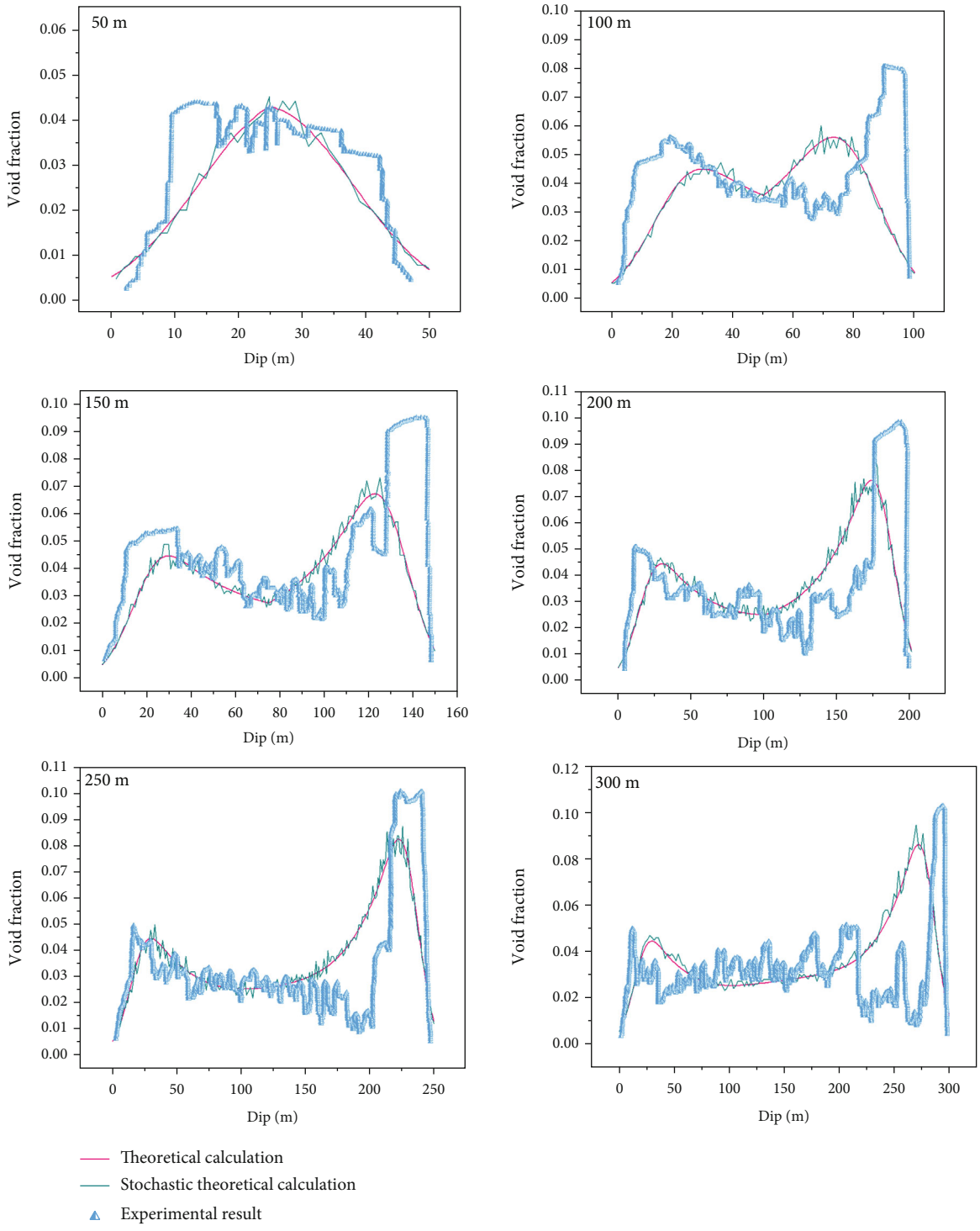

FIGURE 25: Comparison of void fractions for different mining lengths, including theoretical calculations, stochastic calculations, and experimental results.

The overall distribution of void fractions in the disturbed overburden seam shows a double-hump distribution with one high and one low for coal seam inclination angles of 5°, 15°, 30°, 45°, and 60°. The void fraction in the inclination direction undergoes a change from the upper to the lower end, rapidly increasing to a maximum peak, then gradually decreasing, followed by a rapid increase to a second peak, followed by a decrease closest to the lower end. In terms of angular variation, the peak increases as the angle increases, and the void fraction increases significantly at the upper end of the tendency. The peak in void fractions occurs at the upper inward end of the inclination. The stochastic

model better reflects the randomness and dispersion of void fraction after overburden collapse as influenced by dip angle and gravity and is supported by similar simulations.

6.2. Void Fractions for Different Mining Lengths. Combining theoretical calculations, stochastic calculations, and experimental results, the distributions of void fractions in overburden under six different mining lengths of 30° inclined coal seams were compared. The three types of results have good agreement, and the experimental results confirm the accuracies of the theoretical and stochastic calculations. As can be seen from Figure 25, at the excavation length of 50 m, the void fraction distribution curve shows an inverted "V" shape. The void fraction distribution curve gradually turns into a double hump shape with one high and one low at the excavation lengths of 100 m, 150 m, 200 m, 250 m, and 300 m. As the mining length increases, the two peaks of the void fraction distribution curve increase, and the maximum peak appears when the mining length is 300 m. This indicates that as the mining length of the inclined coal seam increases, the scope of the mining-disturbed area expands, the void fraction shows an increasing trend, and the maximum value of void fraction gradually shifts from the middle to near the upper end of the inclination direction. The stochastic model is more consistent with the actual random and discrete characteristics of void fraction distribution than the theoretical determination model and has better practicality.

7. Conclusions

A theoretical calculation model for void fractions in each partition of overburden in inclined coal seam mining that considers the influence of seam inclinations and gravity has been established. Combining similar physical simulation experiments and digital image processing approaches, the stochastic model for characterization of void fraction distributions was obtained.

Void fractions are greatly influenced by the inclination angle of rock seam and mining length. The void fraction in disturbed overburdens above inclined coal seams has a double hump distribution from the upper end to the lower end, and the double peak of the void fraction increases with the increase in seam inclination. With the increase of mining length, void fraction distribution gradually changes from an inverted "V"-shaped distribution to a double-hump distribution with one high peak and other low peak, and the void fraction gradually increases.

The void fraction in the mining-disturbed overlying rock strata gradually decreases from the extraction area towards the ground surface. It gradually decreases from the periphery to the center of the mining-disturbed area. The voids are primarily distributed in the peripheries of the mining-disturbed area, and the upper area of the inclined direction of the overlying strata has richer void.

The experimental results are in good agreement with the theoretically deterministic model and the stochastic model. The stochastic model is developed by combining the theoretical model and the actual situation, which can provide more accurate and effective parameters for understanding the heat and mass transfer during coal fire control, gas extraction, and groundwater control.

Data Availability

The data used to support the findings of this study are included within the article.

Conflicts of Interest

The authors declare no conflicts of interest.

Acknowledgments

This research was supported by the National Natural Science Foundation of China (No. 52174229) and the Natural Science Foundation of Liaoning Province (No. 2021-KF-23-01), for which the authors are very thankful.

References

[1] H. Dai, J. Guo, S. Yi et al., "Stratum and surface movement mechanism in horizontal slicing mining of extremely thick and steep coal seams," *Journal of China Coal Society*, vol. 38, no. 7, pp. 1109–1115, 2013.

[2] Q. Yao, T. Feng, and Z. Liao, "Failure characteristics and movement rule of sublevel filling tendency overburden in steep strike," *Journal of China Coal Society*, vol. 42, no. 12, pp. 3096–3105, 2017.

[3] Y. Zhang, J. Cheng, X. Wang, Z. Feng, and M. Ji, "Thin plate model analysis on roof break of up-dip or down-dip mining stope," *Jounal of Mining & Safety Engineering*, vol. 27, no. 4, pp. 487–493, 2010.

[4] M. Damghani, R. Rahmannejad, and M. Najafi, "Evaluation of the effect of coal seam dip on stress distribution and displacement around the mechanized longwall panel," *Journal of Mining Science*, vol. 55, pp. 733–742, 2019.

[5] M. He, Q. Wang, and Q. Wu, "Innovation and future of mining rock mechanics," *Journal of Rock Mechanics and Geotechnical Engineering*, vol. 13, no. 1, pp. 1–21, 2021.

[6] H. Jangara and C. A. Ozturk, "Longwall top coal caving design for thick coal seam in very poor strength surrounding strata," *International Journal of Coal Science & Technology*, vol. 8, no. 4, pp. 641–658, 2021.

[7] A. A. Ordin and A. M. Nikol'sky, "Optimizing cutting width and capacity of shearer loaders in longwall mining of gently dipping coal seams," *Journal of Mining Science*, vol. 54, no. 1, pp. 69–76, 2018.

[8] J. Wang, W. Wei, and J. Zhang, "Theoretical description of drawing body shape in an inclined seam with longwall top coal caving mining," *International Journal of Coal Science & Technology*, vol. 7, pp. 182–195, 2020.

[9] J. Wang, S. Yang, W. Wei, J. Zhang, and Z. Song, "Drawing mechanisms for top coal in longwall top coal caving (LTCC): a review of two decades of literature," *International Journal of Coal Science & Technology*, vol. 8, no. 6, pp. 1171–1196, 2021.

[10] Y. Wang, M. He, J. Yang et al., "Case study on pressure-relief mining technology without advance tunneling and coal pillars

in longwall mining," *Tunnelling and Underground Space Technology*, vol. 97, article 103236, 2020.

[11] D. Yun, Z. Liu, W. Cheng, Z. Fan, D. Wang, and Y. Zhang, "Monitoring strata behavior due to multi-slicing top coal caving longwall mining in steeply dipping extra thick coal seam," *International Journal of Mining Science and Technology*, vol. 27, no. 1, pp. 179–184, 2017.

[12] Q. Bai and S. Tu, "A general review on longwall mining-induced fractures in near-face regions," *Geofluids*, vol. 2019, Article ID 3089292, 22 pages, 2019.

[13] C. He, W. Lu, W. Zha, and F. Wang, "A geomechanical method for predicting the height of a water-flowing fractured zone in a layered overburden of longwall coal mining," *International Journal of Rock Mechanics and Mining Sciences*, vol. 143, p. 104798, 2021.

[14] Y. Yu, D.-C. Zhao, G.-L. Feng, D.-X. Geng, and H.-S. Guo, "Energy evolution and acoustic emission characteristics of uniaxial compression failure of anchored layered sandstone," *Frontiers in Earth Science*, vol. 10, 2022.

[15] G.-L. Feng, X.-T. Feng, B.-R. Chen, Y.-X. Xiao, and Y. Yu, "A microseismic method for dynamic warning of rockburst development processes in tunnels," *Rock Mechanics and Rock Engineering*, vol. 48, no. 5, pp. 2061–2076, 2015.

[16] D. Xuan, J. Xu, B. Wang, and H. Teng, "Borehole investigation of the effectiveness of grout injection technology on coal mine subsidence control," *Rock Mechanics and Rock Engineering*, vol. 48, no. 6, pp. 2435–2445, 2015.

[17] X. Zhang, R. Y. S. Pak, Y. Gao et al., "Field experiment on directional roof presplitting for pressure relief of retained roadways," *International Journal of Rock Mechanics and Mining Sciences*, vol. 134, article 104436, 2020.

[18] H. Guo, L. Yuan, B. Shen, Q. Qu, and J. Xue, "Mining-induced strata stress changes, fractures and gas flow dynamics in multiseam longwall mining," *International Journal of Rock Mechanics and Mining Sciences*, vol. 54, pp. 129–139, 2012.

[19] L. C. Li, C. A. Tang, X. D. Zhao, and M. Cai, "Block caving-induced strata movement and associated surface subsidence: a numerical study based on a demonstration model," *Bulletin of Engineering Geology and the Environment*, vol. 73, no. 4, pp. 1165–1182, 2014.

[20] L. Ying-ke, Z. Fu-bao, L. Lang, L. Chun, and H. Shen-yong, "An experimental and numerical investigation on the deformation of overlying coal seams above double-seam extraction for controlling coal mine methane emissions," *International Journal of Coal Geology*, vol. 87, no. 2, pp. 139–149, 2011.

[21] J. Cheng, F. Liu, and S. Li, "Model for the prediction of subsurface strata movement due to underground mining," *Journal of Geophysics and Engineering*, vol. 14, no. 6, pp. 1608–1623, 2017.

[22] C. Ö. Karacan, G. S. Esterhuizen, S. J. Schatzel, and W. P. Diamond, "Reservoir simulation-based modeling for characterizing longwall methane emissions and gob gas venthole production," *International Journal of Coal Geology*, vol. 71, no. 2-3, pp. 225–245, 2007.

[23] S. Wang, X. Li, and D. Wang, "Mining-induced void distribution and application in the hydro-thermal investigation and control of an underground coal fire: a case study," *Process Safety and Environmental Protection*, vol. 102, pp. 734–756, 2016.

[24] W. X. Wang, W. H. Sui, B. Faybishenko, and W. T. Stringfellow, "Permeability variations within mining-induced fractured rock mass and its influence on groundwater inrush," *Environmental Earth Sciences*, vol. 75, no. 4, 2016.

[25] J. Zhang and B. Shen, "Coal mining under aquifers in China: a case study," *International Journal of Rock Mechanics and Mining Sciences*, vol. 41, no. 4, pp. 629–639, 2004.

[26] V. Palchik, "Formation of fractured zones in overburden due to longwall mining," *Environmental Geology*, vol. 44, no. 1, pp. 28–38, 2003.

[27] C. Tian, Y. Liu, X. Yang, Q. Hu, B. Wang, and H. Yang, "Development characteristics and field detection of overburden fracture zone in multiseam mining: a case study," *Energy Science & Engineering*, vol. 8, pp. 602–615, 2020.

[28] G. Wang, M. Wu, R. Wang, H. Xu, and X. Song, "Height of the mining-induced fractured zone above a coal face," *Engineering Geology*, vol. 216, pp. 140–152, 2017.

[29] P. Li, X. Wang, W. Cao, D. Zhang, D. Qin, and H. Wang, "Influence of spatial relationships between key strata on the height of mining-induced fracture zone: a case study of thick coal seam mining," *Energies*, vol. 11, no. 1, p. 102, 2018.

[30] P. Liu, H. Q. Liu, Q. Ma, Q. H. Lu, and M. Q. Liu, "Research on evolution rule of inclination fracture field and support technology in close distance and inclined coal seam mining," *Geotechnical and Geological Engineering*, vol. 37, no. 3, pp. 2081–2090, 2019.

[31] X. Wang and H. Li, "Failure height and fracture evolution pattern of overburden rock in fully mechanized cave mining," *Arabian Journal of Geosciences*, vol. 15, no. 5, 2022.

[32] X. He, Y. Zhao, K. Yang, C. Zhang, and P. Han, "Development and formation of ground fissures induced by an ultra large mining height longwall panel in Shendong mining area," *Bulletin of Engineering Geology and the Environment*, vol. 80, no. 10, pp. 7879–7898, 2021.

[33] C. Zhang, Y. Zhao, X. He, J. Guo, and Y. Yan, "Space-sky-surface integrated monitoring system for overburden migration regularity in shallow-buried high-intensity mining," *Bulletin of Engineering Geology and the Environment*, vol. 80, pp. 1403–1417, 2021.

[34] X. Chi, K. Yang, and Z. Wei, "Breaking and mining-induced stress evolution of overlying strata in the working face of a steeply dipping coal seam," *International Journal of Coal Science & Technology*, vol. 8, no. 4, pp. 614–625, 2021.

[35] T. Hong-Sheng, T. Shi-Hao, Z. Cun, Z. Lei, and Z. Xiao-Gang, "Characteristics of the roof behaviors and mine pressure manifestations during the mining of steep coal seam," *Archives of Mining Sciences*, vol. 62, no. 4, pp. 871–891, 2017.

[36] Z. Liao, T. Feng, W. Yu, G. Wu, K. Li, and F. Gong, "Experimental and theoretical investigation of overburden failure law of fully mechanized work face in steep coal seam," *Advances in Civil Engineering*, vol. 2020, Article ID 8843172, 10 pages, 2020.

[37] J. Lou, F. Gao, J. Yang et al., "Characteristics of evolution of mining-induced stress field in the longwall panel: insights from physical modeling," *International Journal of Coal Science & Technology*, vol. 8, no. 5, pp. 938–955, 2021.

[38] W.-H. Yang, X.-P. Lai, J.-T. Cao, H.-C. Xu, and X.-W. Fang, "Study on evolution characteristics of overburden caving and void during multi-horizontal sectional mining in steeply inclined coal seams," *Thermal Science*, vol. 24, no. 6 Part B, pp. 3915–3921, 2020.

[39] Q. Ye, G. Wang, Z. Jia, C. Zheng, and W. Wang, "Similarity simulation of mining-crack-evolution characteristics of

overburden strata in deep coal mining with large dip," *Journal of Petroleum Science and Engineering*, vol. 165, pp. 477–487, 2018.

[40] B. Ghabraie, G. Ren, J. Smith, and L. Holden, "Application of 3D laser scanner, optical transducers and digital image processing techniques in physical modelling of mining-related strata movement," *International Journal of Rock Mechanics and Mining Sciences*, vol. 80, pp. 219–230, 2015.

[41] Y. Sun, J. Zuo, M. Karakus, L. Liu, H. Zhou, and M. Yu, "A new theoretical method to predict strata movement and surface subsidence due to inclined coal seam mining," *Rock Mechanics and Rock Engineering*, vol. 54, no. 6, pp. 2723–2740, 2021.

[42] Y. Liu, Q. M. Liu, W. P. Li, T. Li, and J. H. He, "Height of water-conducting fractured zone in coal mining in the soil–rock composite structure overburdens," *Environmental Earth Sciences*, vol. 78, no. 7, 2019.

[43] Q. Wang, S. Xu, M. He, B. Jiang, H. Wei, and Y. Wang, "Dynamic mechanical characteristics and application of constant resistance energy-absorbing supporting material," *International Journal of Mining Science and Technology*, vol. 32, no. 3, pp. 447–458, 2022.

[44] Q. Wang, S. Xu, Z. Xin, M. He, H. Wei, and B. Jiang, "Mechanical properties and field application of constant resistance energy-absorbing anchor cable," *Tunnelling and Underground Space Technology*, vol. 125, article 104526, 2022.

[45] D. Chen, C. Sun, and L. Wang, "Collapse behavior and control of hard roofs in steeply inclined coal seams," *Bulletin of Engineering Geology and the Environment*, vol. 80, pp. 1489–1505, 2021.

[46] M.-Z. Gao, B.-G. Yang, J. Xie et al., "The mechanism of microwave rock breaking and its potential application to rock-breaking technology in drilling," *Petroleum Science*, 2022.

[47] Y. Wang, H. N. Yang, J. Q. Han, and C. Zhu, "Effect of rock bridge length on fracture and damage modelling in granite containing hole and fissures under cyclic uniaxial increasing-amplitude decreasing-frequency (CUIADF) loads," *International Journal of Fatigue*, vol. 158, article 106741, 2022.

[48] M. Khanal, H. Guo, and D. Adhikary, "3D numerical study of underground coal mining induced strata deformation and subsequent permeability change," *Geotechnical and Geological Engineering*, vol. 37, pp. 235–249, 2019.

[49] Z. Meng, X. Shi, and G. Li, "Deformation, failure and permeability of coal-bearing strata during longwall mining," *Engineering Geology*, vol. 208, pp. 69–80, 2016.

[50] C. Özgen Karacan and G. Goodman, "Hydraulic conductivity changes and influencing factors in longwall overburden determined by slug tests in gob gas ventholes," *International Journal of Rock Mechanics and Mining Sciences*, vol. 46, no. 7, pp. 1162–1174, 2009.

[51] J. A. Wang and H. D. Park, "Coal mining above a confined aquifer," *International Journal of Rock Mechanics and Mining Sciences*, vol. 40, no. 4, pp. 537–551, 2003.

[52] J. Zhang, "Investigations of water inrushes from aquifers under coal seams," *International Journal of Rock Mechanics and Mining Sciences*, vol. 42, no. 3, pp. 350–360, 2005.

[53] J. Cheng, G. Zhao, and S. Li, "Predicting underground strata movements model with considering key strata effects," *Geotechnical and Geological Engineering*, vol. 36, pp. 621–640, 2018.

[54] J. H. He, W. P. Li, Y. Liu, Z. Yang, S. L. Liu, and L. F. Li, "An improved method for determining the position of overlying separated strata in mining," *Engineering Failure Analysis*, vol. 83, pp. 17–29, 2018.

[55] Z. Lou, K. Wang, J. Zang, W. Zhao, B. Qin, and T. Kan, "Effects of permeability anisotropy on coal mine methane drainage performance," *Journal of Natural Gas Science and Engineering*, vol. 86, p. 103733, 2021.

[56] J. Ning, J. Wang, Y. Tan, and Q. Xu, "Mechanical mechanism of overlying strata breaking and development of fractured zone during close-distance coal seam group mining," *International Journal of Mining Science and Technology*, vol. 30, no. 2, pp. 207–215, 2020.

[57] J. A. Vallejos and S. D. McKinnon, "Correlations between mining and seismicity for re-entry protocol development," *International Journal of Rock Mechanics and Mining Sciences*, vol. 48, no. 4, pp. 616–625, 2011.

[58] Z. Tao, Q. Geng, C. Zhu et al., "The mechanical mechanisms of large-scale toppling failure for counter-inclined rock slopes," *Journal of Geophysics and Engineering*, vol. 16, no. 3, pp. 541–558, 2019.

[59] C. Zhu, M. Karakus, M. He et al., "Volumetric deformation and damage evolution of Tibet interbedded skarn under multistage constant-amplitude-cyclic loading," *International Journal of Rock Mechanics and Mining Sciences*, vol. 152, article 105066, 2022.

[60] R. Earon and B. Olofsson, "Hydraulic heterogeneity and its impact on kinematic porosity in Swedish coastal terrains," *Engineering Geology*, vol. 245, pp. 61–71, 2018.

[61] T. Wang, W. Hu, D. Elsworth et al., "The effect of natural fractures on hydraulic fracturing propagation in coal seams," *Journal of Petroleum Science and Engineering*, vol. 150, pp. 180–190, 2017.

[62] D. P. Adhikary and H. Guo, "Modelling of longwall mining-induced strata permeability change," *Rock Mechanics and Rock Engineering*, vol. 48, pp. 345–359, 2015.

[63] H. Guo, D. P. Adhikary, and M. S. Craig, "Simulation of mine water inflow and gas emission during longwall mining," *Rock Mechanics and Rock Engineering*, vol. 42, pp. 25–51, 2009.

[64] S. J. Schatzel, C. Ö. Karacan, H. Dougherty, and G. V. R. Goodman, "An analysis of reservoir conditions and responses in longwall panel overburden during mining and its effect on gob gas well performance," *Engineering Geology*, vol. 127, pp. 65–74, 2012.

[65] S. Wang, D. Elsworth, and J. Liu, "Permeability evolution in fractured coal: the roles of fracture geometry and water-content," *International Journal of Coal Geology*, vol. 87, no. 1, pp. 13–25, 2011.

[66] Z. Pan and L. D. Connell, "Modelling permeability for coal reservoirs: a review of analytical models and testing data," *International Journal of Coal Geology*, vol. 92, pp. 1–44, 2012.

[67] S. Wang and X. Li, "Dynamic distribution of longwall mining-induced voids in overlying strata of a coalbed," *International Journal of Geomechanics*, vol. 17, no. 6, 2017.

[68] S. Wang, X. Li, and D. Wang, "Void fraction distribution in overburden disturbed by longwall mining of coal," *Environmental Earth Sciences*, vol. 75, no. 2, 2016.

[69] S. Wang, X. Li, and S. Wang, "Separation and fracturing in overlying strata disturbed by longwall mining in a mineral deposit seam," *Engineering Geology*, vol. 226, pp. 257–266, 2017.

[70] S. Wang, D. Wang, K. Cao, S. Wang, and Z. Pi, "Three dimensional distribution law of void ratio in goaf and overlying

strata," *Journal of Central South University (Natural Science Edition)*, vol. 45, no. 3, pp. 833–839, 2014.

[71] J. Zhu, *Study on the dimensionless mathematical model and criterion for spontaneous combustion in goaf on the moving coordinate*, China University of Mining and Technology, Beijing, China, 2006.

[72] Z. Ma, *Compaction and seepage characteristics of goaf broken rock*, China University of Mining and Technology Press, Xuzhou, China, 2009.